Mechanisms Controlling the Interannual Variation of Mixed Layer Temperature Averaged over the Niño-3 Region

SEUNG-BUM KIM,* TONG LEE, AND ICHIRO FUKUMORI

Jet Propulsion Laboratory, California Institute of Technology, Pasadena, California

(Manuscript received 16 March 2006, in final form 21 November 2006)

ABSTRACT

Processes controlling the interannual variation of mixed layer temperature (MLT) averaged over the Niño-3 domain (5°N–5°S, 150°–90°W) are studied using an ocean data assimilation product that covers the period of 1993–2003. The overall balance is such that surface heat flux opposes the MLT change but horizontal advection and subsurface processes assist the change. Advective tendencies are estimated here as the temperature fluxes through the domain's boundaries, with the boundary temperature referenced to the domain-averaged temperature to remove the dependence on temperature scale. This allows the authors to characterize external advective processes that warm or cool the water within the domain as a whole. The zonal advective tendency is caused primarily by large-scale advection of warm-pool water through the western boundary of the domain. The meridional advective tendency is contributed to mostly by Ekman current advecting large-scale temperature anomalies through the southern boundary of the domain. Unlike many previous studies, the subsurface processes that consist of vertical mixing and entrainment are explicitly evaluated. In particular, a rigorous method to estimate entrainment allows an exact budget closure. The vertical mixing across the mixed layer (ML) base has a contribution in phase with the MLT change. The entrainment tendency due to the temporal change in ML depth is negligible compared to other subsurface processes. The entrainment tendency by vertical advection across the ML base is dominated by large-scale changes in upwelling and the temperature of upwelling water. Tropical instability waves (TIWs) result in smaller-scale vertical advection that warms the domain during La Niña cooling events. However, such a warming tendency is overwhelmed by the cooling tendency associated with the large-scale upwelling by a factor of 2. In summary, all the balance terms are important in the MLT budget except the entrainment due to lateral induction and temporal variation in ML depth. All three advective tendencies are primarily caused by large-scale and low-frequency processes, and they assist the Niño-3 MLT change.

When the advective tendencies are evaluated by spatially averaging the conventional local advection of temperature, the apparent effects of currents with spatial scales smaller than the domain (such as TIWs) become very important as they redistribute heat within the Niño-3 domain. As a result, for example, the averaged zonal advective tendency counteracts rather than assists the Niño-3 MLT change. However, such internal redistribution of heat does not represent external processes that control the domain-averaged MLT.

1. Introduction

El Niño–Southern Oscillation (ENSO) is a major mode of interannual climate variability in the tropical Pacific that has worldwide climatic and socioeconomic impact. El Niño and La Niña are the oceanic components of ENSO. Numerous studies of El Niño/La Niña events have been conducted using observations (e.g., Picaut et al. 1997; McPhaden 2004), theories (e.g., Schopf and Suarez 1988; Jin 1997), and numerical models (e.g., Zebiak and Cane 1987). The oceanic mixed layer (ML) plays a critical role in the evolution of these events (Zebiak and Cane 1987). The mechanism of the mixed layer temperature (MLT) variation is very complicated, even for the seasonal cycle (Kessler et al. 1998). The present study examines processes governing the interannual variation of MLT in the eastern equatorial Pacific.

The interannual MLT balance at several Tropical Atmosphere–Ocean (TAO) mooring locations has been examined by, for example, Schiller et al. (2000) and

* Current affiliation: Remote Sensing Systems, Santa Rosa, California.

Corresponding author address: Dr. S. B. Kim, Remote Sensing Systems, 438 First St., Suite 200, Santa Rosa, CA 95401.
E-mail: kim@remss.com

DOI: 10.1175/JCLI4206.1

Wang and McPhaden (2001, hereafter WM01). These studies concern local heat budgets at a few equatorial mooring locations as opposed to a balance over the larger equatorial domain pertinent to ENSO. The anomalous warming associated with El Niño/La Niña events typically spans thousands of kilometers zonally and hundreds of kilometers meridionally on both sides of the equator. Because of smaller-scale processes such as tropical instability waves (TIWs), it is by no means clear if the local MLT balance is representative of the balance for large-scale heat content (or averaged temperature) of the eastern equatorial Pacific.

In the context of the local versus large-scale balance, Lee et al. (2004) showed that the spatial average of local zonal advection of temperature within the Niño-3 (5°S–5°N, 150°–90°W) region reflects internal redistribution of heat by TIWs rather than *external* processes that affect the heat content of the region. Consequently, spatial averaging of local zonal advection of temperature results in an anomalous cooling (warming) tendency during the warming (cooling) phase of the 1997–99 El Niño (La Niña). This anticorrelation between zonal advective tendency and temperature change does not describe the large-scale physics that the interannual warming is associated with the eastward movement of warm-pool water (Wyrtki 1975; Picaut et al. 1997). To discern external effects from internal redistribution, Lee et al. referenced temperature fluxes across domain boundaries to the spatially averaged temperature of that domain. As such, for instance, an inflow that is warmer than the average temperature of a region would increase the region's average temperature regardless of how heat is redistributed within the domain. Zonal advection evaluated by such a formulation results in a warming tendency for the Niño-3 region associated with El Niño events, which is consistent with conventional expectation (Wyrtki 1975; Picaut et al. 1997).

In the meridional direction, the eddies in the eastern equatorial Pacific redistribute heat between equatorial and off-equatorial regions (e.g., Hansen and Paul 1984; Wang and McPhaden 1999). The eddy activities are strongest around 2°–3°N (e.g., Halpern et al. 1988) but are weak along the Niño-3 meridional boundaries. Consequently the eddy's contribution to meridional advection is mostly to redistribute heat within the Niño-3 domain. The eddy redistribution is one of three important balance terms in the nonseasonal MLT balance (Vialard et al. 2001). Yet, its significance as an external factor controlling the Niño-3 MLT as a whole is not obvious.

The vertical advective tendency in MLT budget is one of the most poorly understood components of the budget, mainly because its evaluation is difficult [e.g., in observations as noted by Qiu (2002) or in a z-coordinate model (Vialard and Delecluse 1998)]. Consequently, it has often been inferred as a residual of the MLT balance (WM01; Vialard et al. 2001). Yet the residual also contains errors associated with inaccuracies in estimating other terms as pointed out by WM01. Furthermore, budget analysis is complicated by the difficulty in separating the vertical advection from other subsurface processes such as vertical diffusion. Without such separation an assessment of large-scale versus eddy processes among other issues becomes very difficult. Here we use a new discrete equation for the entrainment heat advection (Kim et al. 2006), which allows the closure of MLT budget using output from a z-coordinate model. The rigorous and explicit evaluation of the entrainment heat advection greatly facilitates the analysis of the MLT balance (e.g., Kim et al. 2004). Thus, the rigorous evaluation will be utilized in this study to elucidate the role of the vertical advection in the MLT balance.

To summarize, in this paper we study the processes controlling the Niño-3 MLT in the Niño-3 region by directly evaluating zonal, meridional, and vertical advective contributions for the mixed layer. We adopt two newly developed methods to facilitate the study, namely the evaluation of the external advection of heat (Lee et al. 2004) and a scheme to formally close the MLT budget (Kim et al. 2006). Our analysis is performed for the period of 1993–2003 that encompasses three El Niño/La Niña events (1994–95, 1997–99, and 2002–03). By analyzing the three events we examine how advective tendencies generally contribute to the MLT balance.

This paper is organized as follows. In section 2, we will describe the numerical model output used in this study and evaluate the model fields. Section 3 presents the large-scale balance controlling the averaged MLT of the entire Niño-3 region. In section 4 we address limitations of spatial averages of local advective tendencies to understand processes controlling the Niño-3-averaged MLT. Section 5 summarizes the findings.

2. General circulation model (GCM) products

The analysis fields and temperature budget output used for this investigation are obtained from a data assimilation product called Estimating the Circulation and Climate of the Ocean (ECCO; more information available online at http://www.ecco-group.org). The model used is the parallel version of the primitive equa-

tion Massachusetts Institute of Technology (MIT) ocean GCM (Marshall et al. 1997). The spatial domain is nearly global (80°S–80°N). Horizontal grid spacing is 1° globally except within 20° of the equator, in which meridional grid spacing is gradually reduced to 0.3° within 10° of the equator. There are 46 vertical levels with layer thickness of 10 m in the upper 150 m and 21 layers above 300 m. The model employs two advanced mixing schemes: the K-profile parameterization (KPP) vertical mixing (Large et al. 1994) and the Gent–McWilliams (GM) isopycnal mixing (Gent and McWilliams 1990). The model is forced by the National Centers for Environmental Prediction (NCEP) reanalysis products (12-hourly wind stress, daily heat and freshwater air–sea fluxes) with the time means replaced by those of the Comprehensive Ocean–Atmosphere Data Set fluxes (da Silva et al. 1994). In addition to this imposed heat flux, model sea surface temperature (SST) is relaxed to NCEP's SST analysis with a time scale of 1–2 months using the formulation of Barnier et al. (1995). The model was first spun up for 10 yr from rest using climatological temperature and salinity (Boyer and Levitus 1998) forced by seasonal climatological forcings averaged from 1980 to 1997. Additional descriptions of the model and comparison with various observational data are provided by Lee et al. (2002). An approximate Kalman filter and smoother (Fukumori 2002) are used to assimilate anomalies of sea level and of subsurface temperature obtained from the Ocean Topography Experiment (TOPEX)/Poseidon (T/P) altimeter and the Global Telecommunication System (GTS; D. Behringer 2002, personal communication), respectively. The assimilation procedure corrects the temporal variability of the prior NCEP wind forcing through inversion by the smoother, but does not correct the time-mean wind or, consequently, the model's time-mean state. An earlier version of this system can be found in Fukumori et al. (1999). The modification of the wind forcing, although small in many regions, is effective in bringing the model closer to the data that are being assimilated. A detailed description of the principle of the Kalman filter and smoother approach can be found in Fukumori (2006). The resultant analysis fields are consistent with the physics of the GCM such that the property budgets (heat, salt, and momentum) are closed. A previous example of applying this product to study MLT balance is provided by Kim et al. (2004) for the north-central Pacific.

To assess the fidelity of the assimilation product, we first evaluate the mixed layer depth. Then we examine the model's temperature and velocities at the equator, along with the simulated properties at the Niño-3 boundaries. The properties at the boundaries are important to the characterization of external processes controlling the Niño-3 MLT.

The ML is determined diagnostically from the GCM output fields such that the density at the ML depth is larger than that at 5 m (i.e., the model's surface level) by 0.125 kg m^{-3}. The density offset corresponds to a 0.5-K temperature difference between sea surface and ML base at 35 psu and 20°C, which is a commonly used criterion for the ML in the Tropics (e.g., Hayes et al. 1991; WM01). The isothermal layer depths derived from expendable bathythermograph (XBT) observations and the model compare reasonably well with each other (Fig. 1a), demonstrating the fidelity of the model estimates. On average, the model's isothermal layer is too shallow by 6 m. This may be due to the mixing coefficient in the model being too small. The smaller range of temporal variability may also be due to an underestimate in the variability in wind discussed later. In this area, unlike regions to the west (Lukas and Lindstrom 1991), a barrier layer is not so common and isothermal layer depth and ML depth are almost identical (Fig. 1a). The most noticeable change in the ML depth is the shoaling during the La Niña in 1998 (Fig. 1b).

Figures 2–5 compare the estimated temperatures and velocities between simulation and observation at the TAO mooring locations at 5°N, 0°, and 5°S latitude and at 140° and 110°W longitude. The velocity comparison is performed only at the equator where current meters are available. Hereafter, "simulation" or "model" refers to the data assimilation product, not to be confused with the model simulation prior to data assimilation. The data and the model fields are averaged over 10 days and are sampled at depths around 10 and 45 m, the depths that are mostly within the ML except at 0°, 110°W, where the ML depth is 22 ± 8 m (time mean and standard deviation). The model fields are interpolated horizontally and vertically to collocate with the data. Temperature and velocity are both reasonably well simulated at all TAO mooring locations. The warming and cooling in 1997 and 1998 as well as the eastward current anomalies in spring and winter 1997 and the westward anomaly in spring 1998, both associated with the El Niño and La Niña, respectively, are reasonably captured by the simulation. However, as noted above, the assimilation does not correct time-mean model biases. At the equator, the temperature within the ML (10 and 45 m at 140°W, 10 m at 110°W) has an average cold bias of 1.3 K. The cold bias is common in ocean numerical models but its detailed causes are not well understood (Jochum et al. 2005). Zonal velocity at 110°W, 45-m depth has a bias of 44

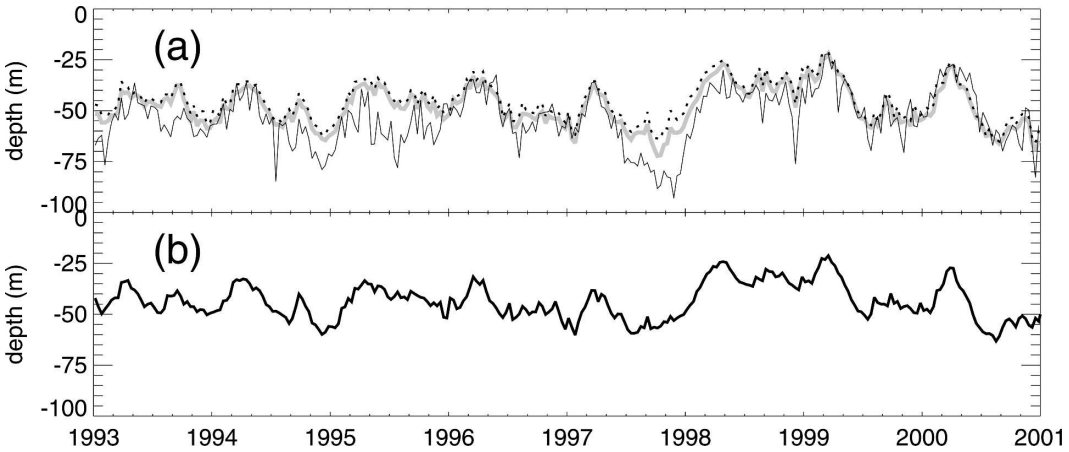

FIG. 1. (a) Comparison of the model isothermal layer depth (ILD, thick gray) over the Niño-3 area with XBT ILD (thin black) at the locations where XBTs are available. The model's mixed layer depth (MLD) is shown in black dots. The ILD (MLD) is determined such that the temperature (density) at the layer base is lower (larger) than the 5-m value by 0.5 K ($0.125\sigma_\theta$). (b) Domain-mean MLD from the model with even spatial sampling. All the depth values are given every 10 days.

cm s^{-1}, which reflects the model's excess shoaling of the mean depth of the Equatorial Undercurrent, which may also be due to inaccuracies in vertical mixing as in biases of ML depth.

The model's corresponding wind estimates are compared with observations in Fig. 6. Both zonal and meridional components are reasonably estimated, but the zonal component is somewhat more accurately esti-

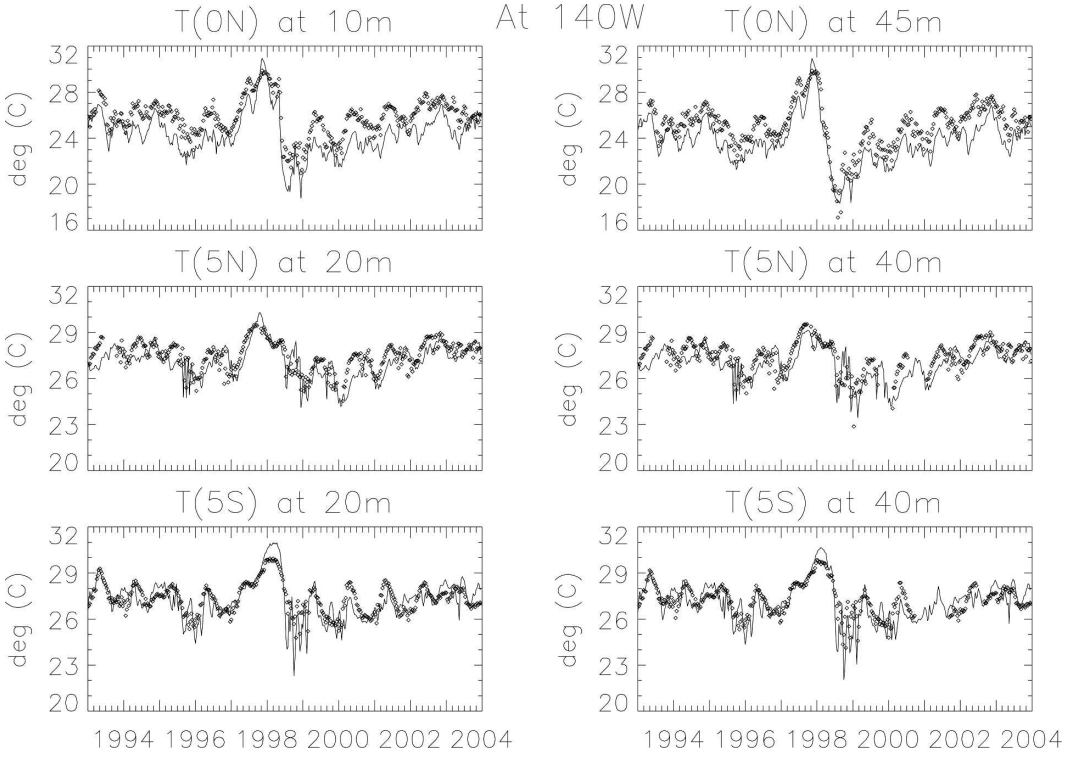

FIG. 2. Comparison of model temperatures (solid line) and observations at TAO locations (dots) at 140°W in the Niño-3 area. Temperatures at (top) 0°, (middle) 5°N, and (bottom) 5°S are compared. To sample within an ML, the comparison is performed at TAO nominal depths at (left) 10–20 and (right) 40–45 m. The simulated and observed time series are averaged over 10 days.

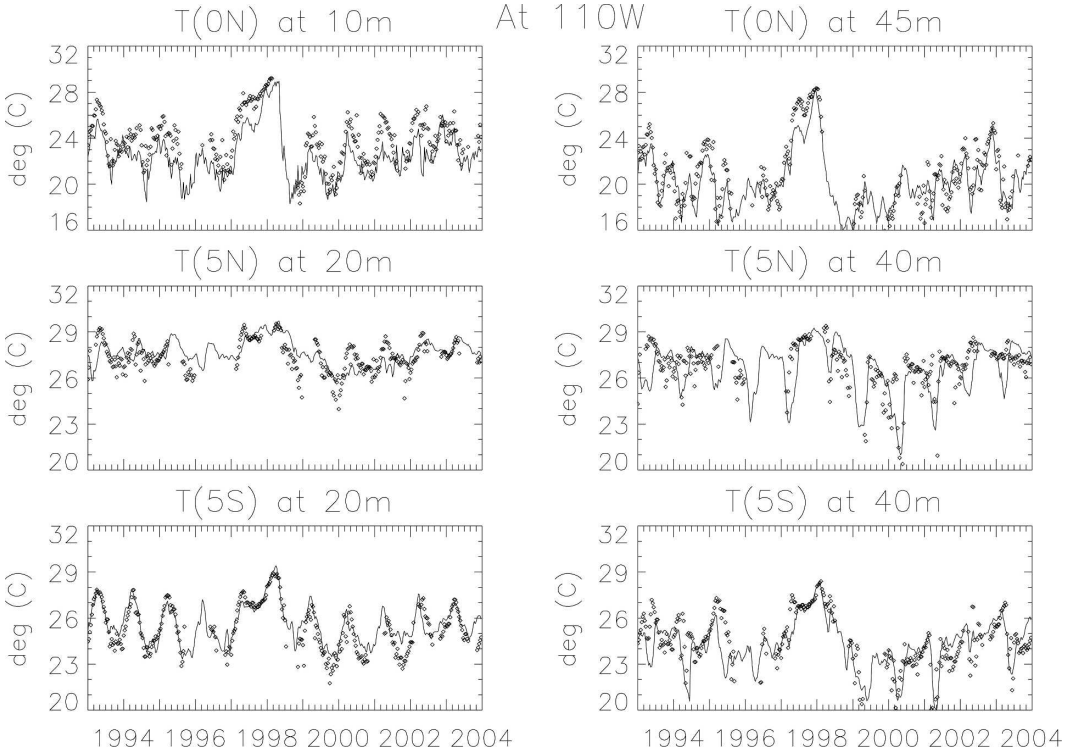

FIG. 3. Same as in Fig. 2, but for 110°W in the Niño-3 area.

mated than the meridional winds. This difference reflects the accuracy of the NCEP reanalysis on the one hand and the sensitivity of the assimilation on the respective wind components on the other. Zonal wind anomalies affect large-scale sea level and temperature anomalies more than do meridional wind anomalies.

The temporal variabilities of temperature and velocity are comparable to observations, but in general the latter is not as accurately simulated as the former relative to their respective variabilities. This difference is partly due to the shorter spatial correlation distance of velocity fluctuations compared to temperature variability on the one hand and the relatively coarse spatial resolution of the present model on the other. In particular, equatorial meridional velocities are dominated by high-frequency signals associated with TIWs (Figs. 4c,d and 5c,d; e.g., Halpern et al. 1988). The periods of the year when TIWs are active (boreal fall and winter) are well simulated, but the particular high-frequency fluctuations are generally incoherent with observations, reflecting the unstable nature of TIWs. Moreover, the model underestimates the magnitude of meridional velocity fluctuation by about 50%. According to Jochum et al. (2005), ¼° horizontal resolution is sufficient for simulating TIWs while 1°, as in our model's zonal resolution, is not. The magnitude of the meridional velocity is sensitive also to the viscosity (Cox 1980), and the mixing could be another reason for the weak simulated TIWs.

The model's discrepancies with observations do not seem to influence the fidelity of the estimated MLT budget at the equator. In particular, the pointwise MLT balance at the equator inferred from the model fields is consistent with the observational analysis of WM01 (appendix A). The relative agreement between the model states and observations and the consistency of the pointwise budget provides confidence in analyzing the present model estimate to study the MLT balance over the Niño-3 region.

Finally, the advective tendency that controls the Niño-3-averaged MLT is determined by temperature and velocity at Niño-3 boundaries, as we will show in section 3. No current meter measurement is available at the TAO mooring locations along the Niño-3 boundaries, so assessing the accuracy of the model's total current is difficult. Yet a significant portion of meridional flow across 5°N and 5°S within the ML is Ekman transport. Above 50-m depth along these boundaries Ekman currents account for more than two-thirds of meridional transport in terms of time-mean and interannual variability [Fig. 9 of Bryden and Brady (1985) and Fig. 4 of Meinen et al. (2001), respectively]. Then a com-

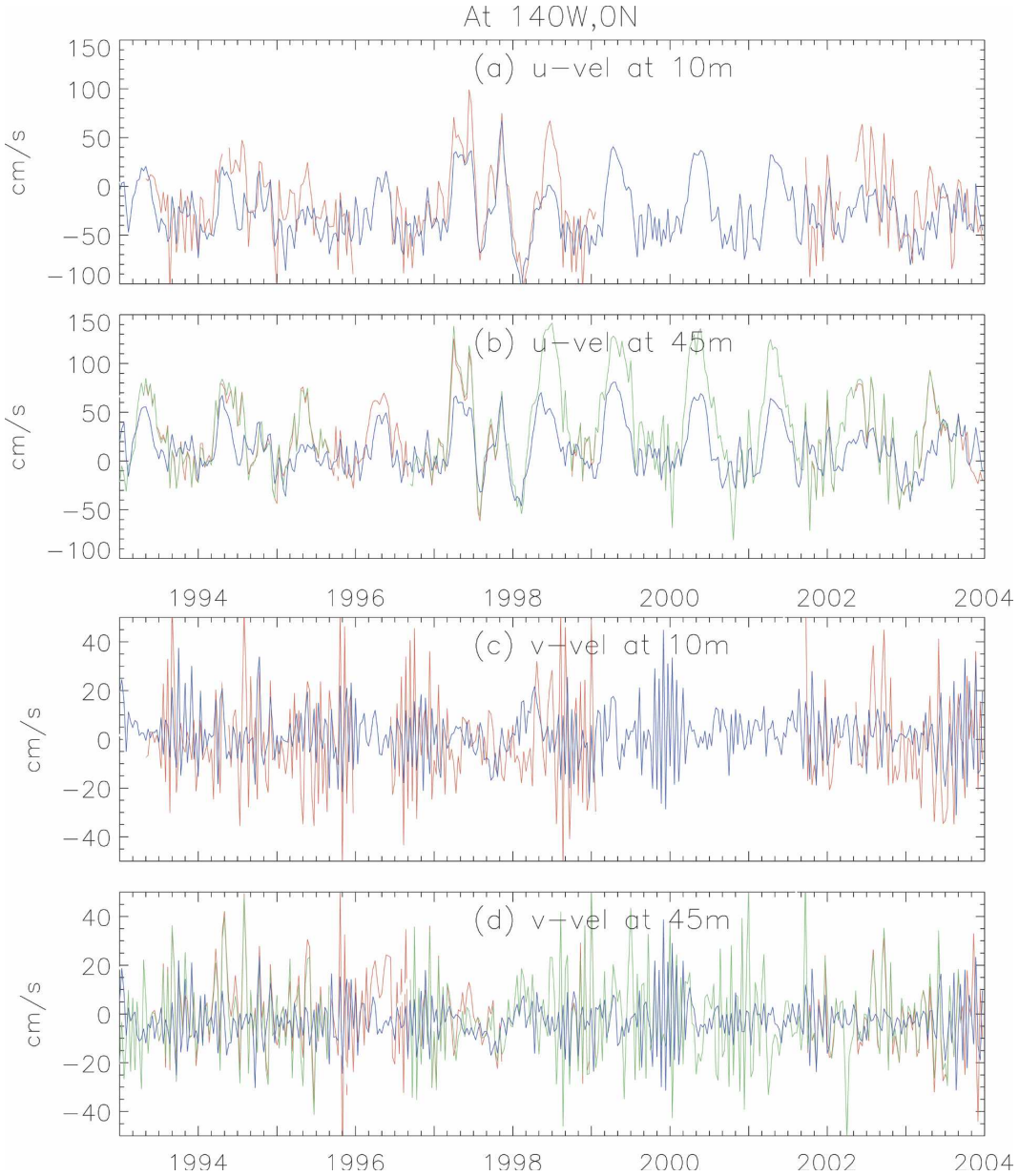

FIG. 4. Comparison of model velocities (blue) and observations at TAO locations (red for current meter records and green for ADCP records) at 0°, 140°W at two depth levels: (a), (b) zonal velocities and (c), (d) meridional velocities. The simulated and observed time series are averaged over a 10-day interval. The time span for ADCP records at 10 m is not long thus the data are not plotted.

parison of zonal wind along 5°N and 5°S would be useful for assessing the model's meridional velocity. Figure 7 shows that model's zonal winds at these latitudes agree well with the measurements obtained from the European Remote Sensing satellite scatterometers. The corresponding temperatures from the model at 5°N and 5°S, 140° and 110°W also show good agreement with observations both in phase and magnitude (Figs. 2 and 3). These agreements in velocity and temperature further strengthen our confidence in the model's meridional temperature flux across the northern and southern boundaries of the Niño-3 region.

3. Processes controlling the Niño-3 domain-averaged MLT

The equation describing the balance of the spatially averaged MLT change can be given as (Kim et al. 2006)

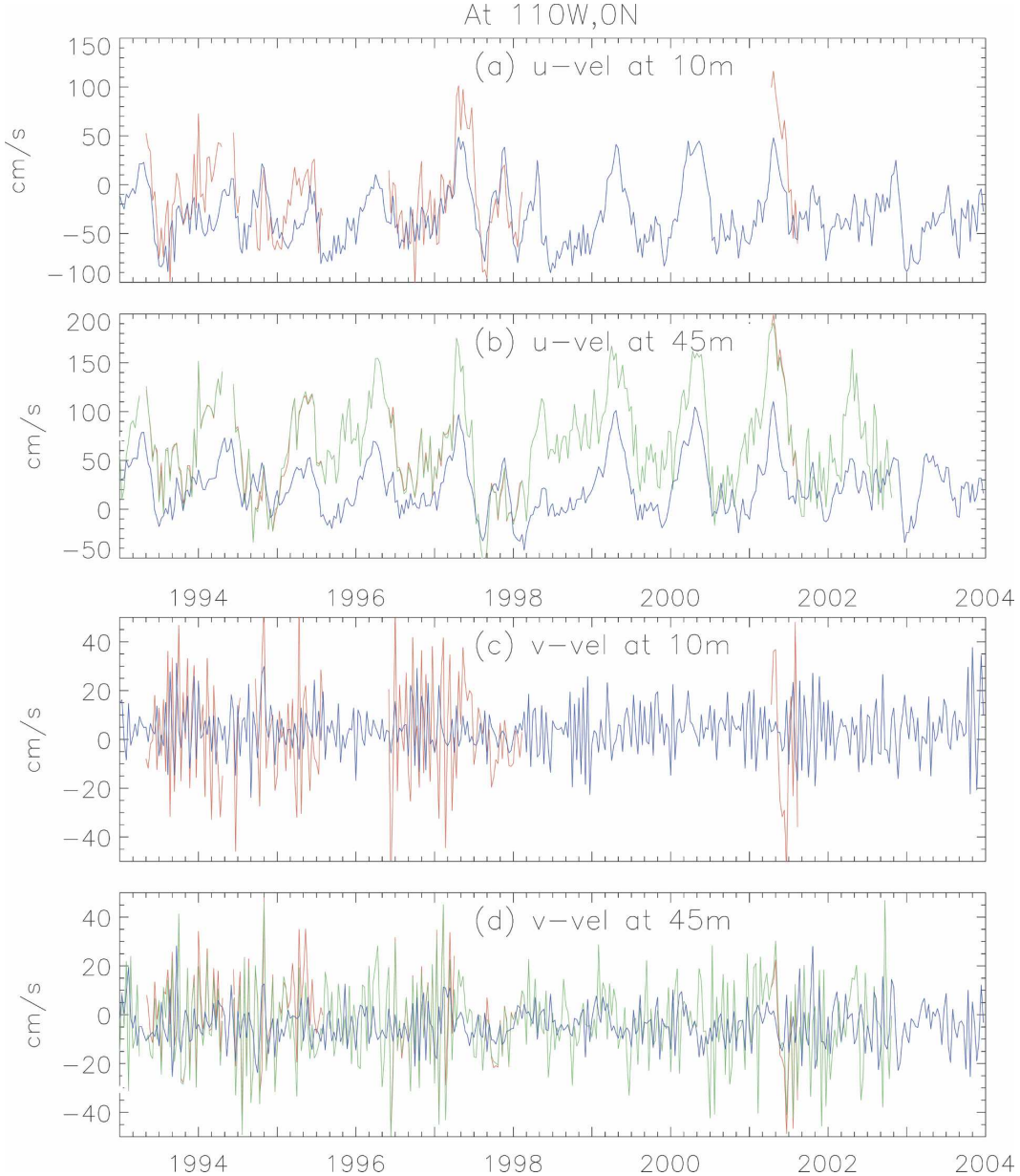

FIG. 5. Same as in Fig. 4, but for 0°, 110°W.

$$\frac{d\langle T\rangle}{dt} = \left\langle \frac{1}{\rho C_p}\frac{\partial q}{\partial z}\right\rangle + \langle \nabla_z(\kappa \nabla_z T)\rangle_{z=0} - \{u_\perp (T - T_r)\}_{\mathrm{ML}} + \text{subsurface} + \langle \text{ML mixing}\rangle, \quad (1a)$$

$$\text{subsurface} = \left\langle \frac{1}{h}\Delta T \frac{\partial h}{\partial t}\right\rangle - \{u_\perp (T - T_r)\}_{\text{induct}} - \{w(T - T_r)\} + \langle \nabla_z(\kappa \nabla_z T)\rangle_{z=-h}, \quad (1b)$$

$$\Delta T = \langle T\rangle - T_{-h}, \quad (1c)$$

where the angle brackets represent the volume-weighted average over the Niño-3 ML and the braces indicate an integral over ML boundary surfaces after dividing by ML volume. Variables T, h, ρ, and κ are temperature, ML depth, density, and vertical diffusivity, respectively; q is the penetrative solar flux, and C_p is the specific heat of seawater. Also, $u_\perp$ and w are the velocities normal to ML boundaries in horizontal and vertical directions, respectively; $\nabla_z = \partial/\partial z$, and ΔT is the temperature difference between ML water and entrained water. The subscript r denotes a reference. Specifically, $T_r \equiv \langle T\rangle$ and is the volume-averaged MLT

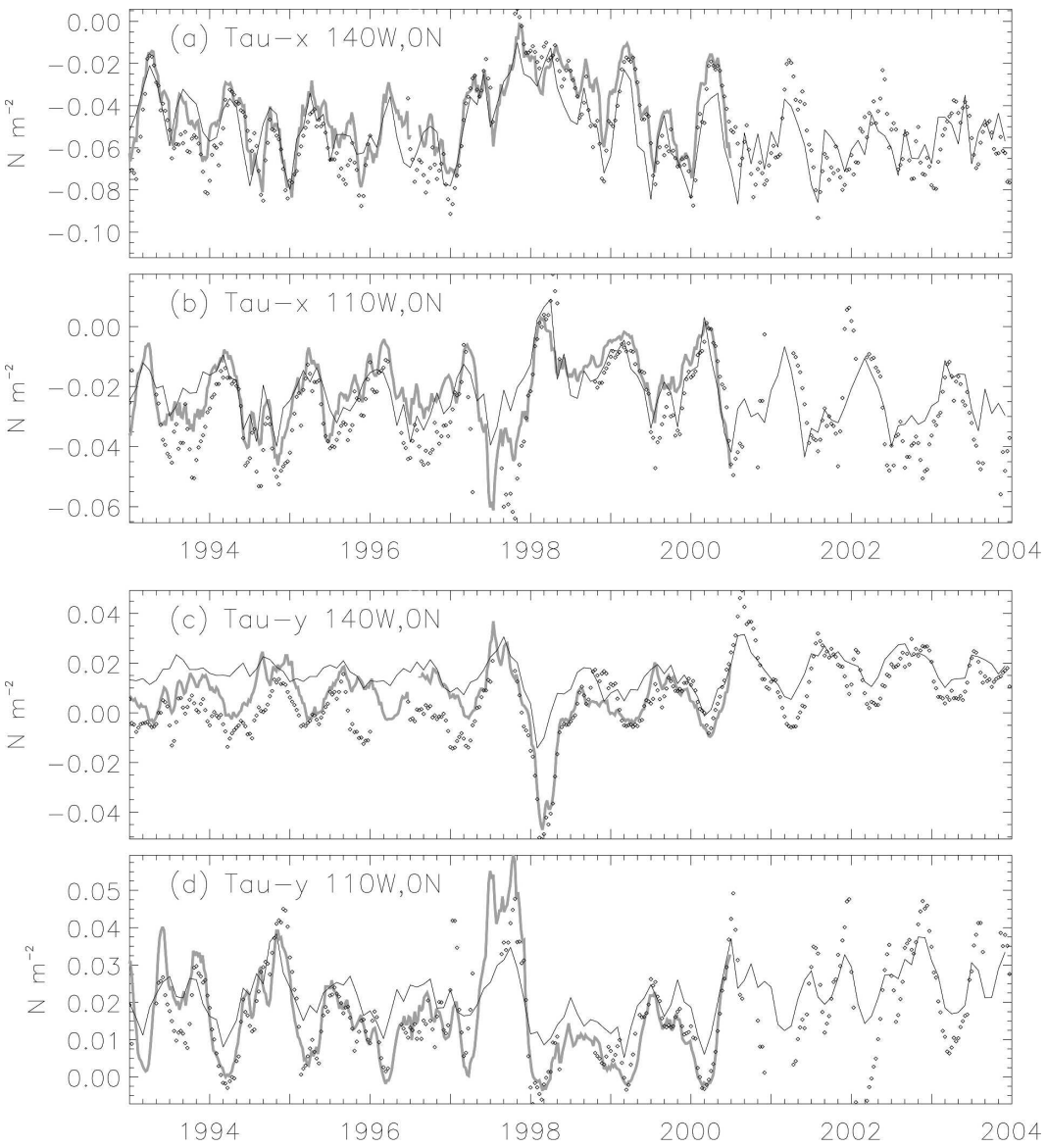

FIG. 6. Comparison of the model wind forcing (thin black) with observations by buoys (dots) and ERS scatterometer (thick gray) at 0°, 140°W and at 0°, 110°W: (a), (b) zonal and (c), (d) meridional components. The time series are averaged over a 30-day interval.

over the Niño-3 region at time t that permits assessing advective contributions from independent directions (Lee et al. 2004). The subscripts ML and induct denote, respectively, the advective tendencies across lateral boundaries within the ML and between the ML and the thermocline (lateral induction).

The components of the rhs of Eq. (1a) define the tendencies by surface heat flux, advection by horizontal currents, subsurface processes, and ML mixing, respectively. The subsurface processes are divided into entrainment heat advection and vertical mixing [Eq. (1b)]. The entrainment heat advection consists of temporal ML depth variation ($\Delta T \partial h/\partial t$), lateral induction, and vertical advection ($-\{w(T - T_r)\}$). The vertical mixing, $\langle \nabla_z(\kappa \nabla_z T)\rangle$, may be expanded as $\int\int[\kappa \nabla_z T(z = 0) - \kappa \nabla_z T(z = -h)]\, dx\, dy/V$ with V denoting the ML volume. The first term is the surface boundary condition and is the sum of outgoing longwave, sensible, and latent heat fluxes $[\langle \nabla_z(\kappa \nabla_z T)\rangle_{z=0}]$. The second term is the vertical mixing at the ML base $[\nabla_z(\kappa \nabla_z T)\rangle_{z=-h}]$. The last term in Eq. (1a), ML mixing, refers to the effect of mixing that is other than the vertical mixing across the ML base. This effect includes the contribution by the GM mixing (more or less horizontal in nature) and the

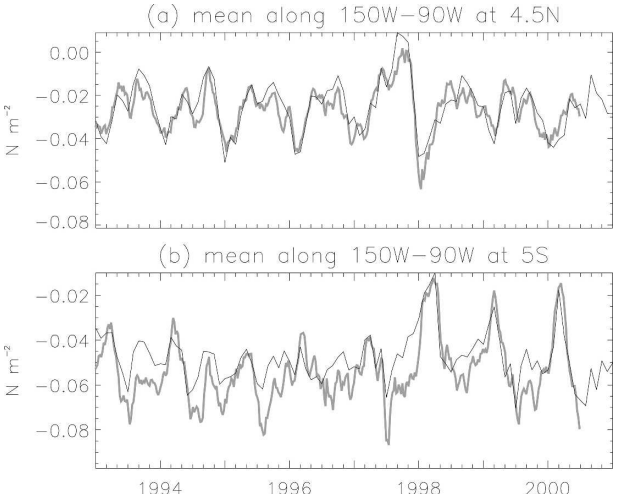

FIG. 7. Comparison of the simulated zonal wind stress (thin black) with respect to ERS scatterometer wind stress (thick gray) along the (a) northern and (b) southern boundaries of the Niño-3 domain. The simulated and ERS winds are averaged over a 30-day interval.

so-called nonlocal transport associated with the KPP vertical mixing.

The formulation of our MLT budget analysis [as described in Eq. (1)] has two improvements when compared to previous analyses of the Niño-3 MLT balance based on z-coordinate model output (e.g., Vialard et al. 2001). First, our formulation is characterized by the closure of the budget, made possible by a direct evaluation of the entrainment component ($\Delta T \partial h/\partial t$). Kim et al. (2006) achieved the closure through rigorous determination of ΔT by using a discrete form based on the numerical model's temperature evolution and by including an apparent warming tendency during ML shoaling to account for the small gradient in the vertical temperature profile within the ML (i.e., detrainment). The second improvement is the use of a modified boundary flux formulation proposed by Lee et al. (2004) to evaluate the advective processes that affect the Niño-3 MLT. The advective term as shown in Eq. (1a), $\{u_\perp(T - T_r)\} + \{w(T - T_r)\}$, is equal to $\{u_\perp T\} + \{wT\}$ because $\{u_\perp T_r\} + \{wT_r\}$ vanishes due to nondivergence, $\{u_\perp\} + \{w\} = 0$. Therefore, the modified boundary flux form $\{u_\perp(T - T_r)\} + \{w(T - T_r)\}$ is identical to the conventional boundary flux form $\{u_\perp T\} + \{wT\}$ when integrated over the entire boundary surfaces of the Niño-3 ML domain. For a partial boundary such as the west face of the Niño-3 domain, the conventional temperature flux through it is not meaningful because of the dependence on the definition of zero temperature. With the modified boundary flux form, the boundary temperature is referenced to the domain-averaged temperature, T_r, and thus the dependence on the definition of zero temperature is removed. Only water advected across the boundary with different temperature from T_r affects the volume mean temperature. Therefore the modified boundary flux form allows analysis of temperature advection through individual boundary surfaces of a domain.

The individual tendencies are evaluated and saved as 30-day integrals during model integration, except the quadratic terms involving domain mean temperature T_r. Since domain mean temperature is dependent on specific volumes, terms $\{u_\perp T_r\}$ and $\{wT_r\}$ are evaluated offline based on 10-day-averaged velocity and temperature time series archived during the simulation. Since T_r slowly varies in time, discrepancies arising from ignoring shorter time-scale correlation between the velocities and T_r are small as evidenced in comparisons with states saved as 1-day averages (not shown). Since our interest is interannual balance, we compiled mean seasonal cycles of tendencies during the 1993–2003 period and removed the mean from the tendencies (see appendix B for the details of the seasonal budget). The resultant quantities are referred to as nonseasonal tendencies.

MLT balance is often presented in tendency space (i.e., tendency as a function of time; e.g., WM01). The tendencies usually have high-frequency signals that complicate interpretation. For this reason, WM01 used a 5-month low-pass filter for the tendencies in order to highlight low-frequency signals. Moreover, to capture the effect of a particular tendency during a certain event or period, one has to visually integrate the tendency in time. To alleviate these complications, we present MLT balance by integrating each tendency term in time starting from January of 1993, the beginning of the study period (Fig. 8). The curves in Fig. 8 are then in temperature space (K) instead of tendency space (K s^{-1}). The slope of a curve now represents the tendency. The change in temperature space over a certain period gives an indication of how important a particular tendency is during that period. The low-frequency signals are more evident in temperature space than in tendency space. The magnitude of each MLT balance component in temperature space is also tabulated in Table 1 for the 1997–98 El Niño/La Niña event.

Surface heat flux cools the ocean during the three El Niños (late 1994, 1997–98, and 2002, Fig. 8a). The opposite happens during the La Niña events. This damping effect of surface heat flux is consistent with the finding of WM01. They attributed the anomalous cooling effect by surface heat flux during El Niño events to the reduced shortwave radiation into the ocean associ-

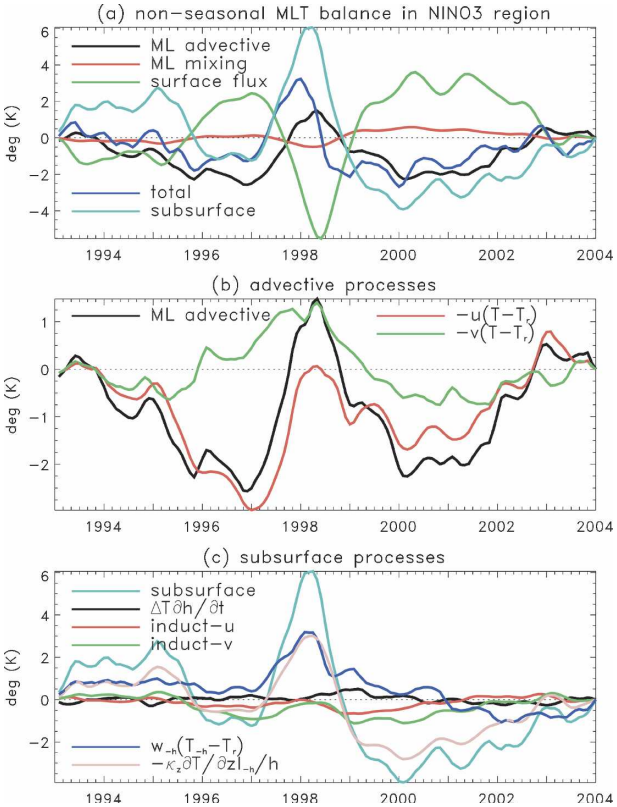

FIG. 8. Nonseasonal MLT balance over the Niño-3 area: (a) overall balance, (b) advective processes within a ML, and (c) subsurface processes. Each curve is a time integral of the component of the nonseasonal MLT tendency, defined in Eq. (1). The advective tendencies are computed using the modified boundary flux form. See Eq. (1) for notations. The tendencies are computed hourly, averaged over 30 days, and smoothed with three-point (90 days) running mean.

ated with increasing cloudiness and greater latent heat loss due to higher SST, and vice versa for La Niña events. The GM mixing, which includes horizontal mixing, and the KPP nonlocal mixing are relatively small (Fig. 8a and Table 1; these two terms are shown together as ML mixing).

The warming and cooling by zonal advection during the El Niños and La Niñas (Fig. 8b), respectively, agree with conventional understanding, that is, eastward intrusion of warm-pool water during an El Niño and westward retreat during a La Niña (Wyrtki 1975; Picaut et al. 1997). The zonal advection contributes about a 3-K warming during the 1997–98 El Niño to the MLT balance (Table 1). Its magnitude is comparable to the total MLT change during the event. Thus, the zonal advection is one of the important factors of the Niño-3 MLT changes. The meridional advective tendency is also in phase with the MLT tendency, the details of which will be discussed later in this section.

We now discuss subsurface processes (Fig. 8c). Vertical advective tendency through the ML base, $w_{-h}(T_{-h} - T_r)$, has the same phase as the MLT variations. Analyzing the 1997–99 El Niño/La Niña, both interannual changes in upwelling rate (w_{-h}) and temperature difference across the ML base ($T_{-h} - T_r$) contribute to the vertical advective tendency. During the El Niño, the upwelling weakens in response to waning trade wind, and depressed thermocline raises the temperature of upwelling thermocline water (T_{-h}) more than the rise of the domain mean temperature (T_r) (not shown). The opposite happens during the La Niñas. Vertical mixing produces warming tendency during the El Niños, and vice versa during the La Niñas. As the thermocline deepens in the cold tongue region during the El Niños, the vertical temperature gradient decreases, and the vertical mixing at the ML base, $-\kappa\partial T/\partial z|_{z=-h}/h$, produces an anomalous warming. Generally the vertical mixing tendency has the same phase as the MLT tendency (Fig. 8c).

Entrainment tendency caused by the variation of ML depth, $\Delta T\partial h/\partial t/h$, contributes to slight warming during

TABLE 1. The time integral of Niño-3 MLT tendency components for the 1997–99 El Niño/La Niña (also shown in Fig. 8). Units are K.

Tendency component	Warming period (Jan 1997–Dec 1997)	Cooling period (Jan 1998–Dec 1999)
MLT	4.20	−5.91
Surface heat flux	−5.16	5.48
KPP + GM mixing	−0.54	0.94
Horizontal advection across domain boundaries within a mixed layer	3.23	−2.98
Zonal	2.74	−1.37
Meridional	0.49	−1.61
Subsurface processes	6.67	−9.35
$\Delta T\partial h/\partial t/h$	−0.13	0.14
Lateral induction (zonal)	0.37	−0.47
Lateral induction (meridional)	0.70	−0.84
Vertical advection	2.53	−2.72
Vertical mixing	3.20	−5.46

the 1998 La Niña but is negligible relative to other subsurface tendencies (Table 1). This warming may be understood with the plots of ΔT, $\partial h/\partial t$, and $\Delta T \partial h/\partial t/h$, presented in Fig. 4 of Kim et al. (2006), where they used the same assimilation product as in this paper. In spring 1998, the ML shoals from about 45- to 25-m depth, shedding off slightly colder water in the deeper part of the original ML. Thus, the shedding results in a higher MLT (i.e., an apparent warming effect). This warming effect is enhanced by ΔT being more positive than normal in spring 1998 (Fig. 4 of Kim et al. 2006). A similar warming is found in springs of 1995 and 2003, but its magnitude is very small (Fig. 8c). Entrainment by lateral induction is not a major term in the MLT balance (Table 1). It is not straightforward to interpret the variability of the lateral induction tendency because of the complicated geometry of the lateral interfaces that are defined by horizontal variations in mixed layer depth.

In general, advective tendencies are contributed by large-scale, low-frequency variations as well as high-frequency fluctuations in the flow and/or temperature fields. In the study region, TIWs that have a dominant 20-day period are a major source of the high-frequency variability. To distinguish the relative contribution of large-scale, low-frequency variability from that of TIWs, we compare the advective tendencies computed from temperature and velocity fields at every time step of the model (hourly) with those estimated from 30-day-averaged temperature and velocity. The 30-day average effectively filters out TIWs. Figure 9 presents such a comparison for zonal, meridional, and vertical advection, respectively. Large-scale processes dominate the zonal advective tendency (Fig. 9a), shown by the very close match between hourly and 30-day evaluations. The importance of large-scale variability is shown most clearly for the 1997–99 El Niño/La Niña event. Most of the zonal advective tendency is contributed by the flux through the western boundary, indicating the large-scale zonal movement of the warm-pool water in response to the variation of the trade wind. The same mechanism applies to the 1994–95 and 2002–03 events but with smaller magnitudes.

The meridional advective tendency is also associated primarily with large-scale fluctuations in temperature and velocity (Fig. 9b), again judging from the relative insensitivity of the tendency to the 30-day averaging. The tendency is contributed mostly by the flux through the southern boundary. Furthermore, the advection of nonseasonal temperature anomalies by seasonal currents is dominant [$\bar{v}_s(T'_s - T'_r)$ during the 1997–99 El Niño/La Niña, Fig. 10, where subscript s denotes values at the southern boundary]. The following provides additional explanation. The $\bar{v}_s$ is southward, consisting

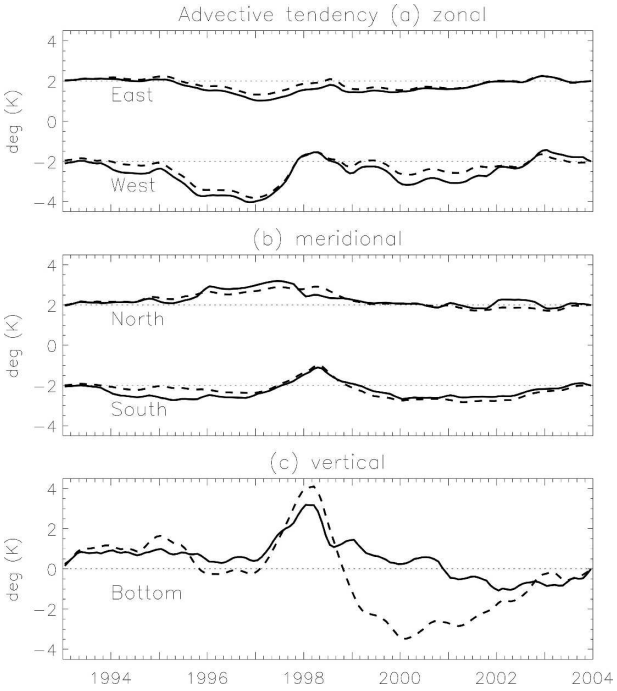

FIG. 9. The time integral of nonseasonal advective tendencies through five boundaries of the Niño-3 domain: (a) zonal, (b) meridional, and (c) vertical. The tendencies are evaluated at two temporal resolutions: hourly (solid) and 30 daily (dashed). All the tendencies are smoothed using the three-point running mean (90 days). For improved presentation, the contributions through the two boundaries in (a), (b) are plotted with an offset value. The level dotted lines indicate the zero reference.

mainly of Ekman currents driven by the trade wind. During the El Niño, the Niño-3-averaged MLT (T'_r) rises more than the temperature along the southern boundary (T'_s), therefore ($T'_s - T'_r$) is negative. Conse-

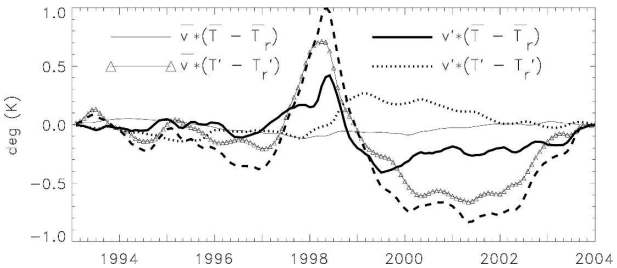

FIG. 10. Decomposition of the nonseasonal meridional advective tendency through the south boundary, shown as dashes in Fig. 9b and in this figure, into ones by the mean seasonal (overbar) and the nonseasonal anomaly (prime) components of temperature (T) and velocity (v). The time integral and three-point running mean are applied to the tendencies. The subscript r denotes a domain-mean reference. The v and T fields are 30-day averages. The thin solid line is not strictly zero because of the division by the time-varying Niño-3 volume.

quently there is a warming contribution by $\overline{v}_s(T'_s - T'_r)$ during a El Niño, and vice versa during the La Niña. Both $\overline{v}_s$ and $(T'_s - T'_r)$ are governed by large-scale dynamics, as is the consequent meridional advective tendency. The tendencies by the anomaly current in Fig. 10, $v'_s(\overline{T}_s - \overline{T}_r)$ and $v'_s(T'_s - T'_r)$, tend to cancel each other, suggesting that they are probably artifacts of the decomposition. The warming tendency by $v'_s(T'_s - T'_r)$ is somewhat counterintuitive because in this La Niña period both v'_s and $(T'_s - T'_r)$ are generally negative. Yet closer examination shows that $(T'_s - T'_r)$ in the far-western region along 5°S turns out to be positive, leading to the warming effect. The tendency through the northern boundary does not seem to have a consistent pattern in time. The slopes of the hourly and 30-daily curves of the north boundary tendency are similar most of the time. This similarity indicates that, overall speaking, TIWs do not play a major role in the meridional advection through the northern boundary either.

Compared to the zonal and meridional advection, the vertical advective tendency is affected by TIWs more significantly (Fig. 9c). For example, the cooling by the vertical advection during the 1998–99 La Niña corresponds to the MLT decrease of about 3 K (solid curve; Table 1). When the TIWs are filtered out from temperature and velocity through the 30-day average, the MLT decreases by about 7 K (dashed curve). In other words, the 7-K cooling by large-scale, low-frequency upwelling is counteracted by a 4-K warming due to the TIWs. Therefore, the magnitude of TIW-induced vertical advective heating is approximately half of that due to large-scale cooling. TIW-induced warming effects through vertical advection are not unique to the tropical Pacific Ocean. In a modeling study of the tropical Atlantic, Jochum et al. (2004, their Fig. 15) also found a time-mean warming tendency due to TIW-induced vertical eddy flux at the depth of 20 m.

The time frame of this study covers three El Niño/La Niña events: 1994–95, 1997–99, and 2002–03. The balance mechanism appears very similar among these three warming–cooling events (Fig. 8). The overall balance is such that surface heat flux opposes the MLT change while horizontal advection and subsurface processes assist the MLT change. Only the magnitude of each term is different from one El Niño/La Niña event to another.

4. Comparison with spatially averaged local temperature advection

Here we present the balance of the volume-averaged MLT changes using a conventional formulation for advective contributions, that is, by spatially averaging local advection of temperature (the product of local velocity and spatial gradient of temperature). The purpose is to compare the balance mechanism with that inferred from the modified boundary flux approach presented in section 3. The conventional formulation is expressed as (e.g., Vialard et al. 2001)

$$\frac{d\langle T\rangle}{dt} = \left\langle \frac{1}{\rho C_p}\frac{\partial q}{\partial z}\right\rangle + \langle \nabla_z(\kappa \nabla_z T)\rangle_{z=0} - \langle (u,v)\cdot \nabla_H T\rangle + \text{subsurface} + \langle \text{ML mixing}\rangle$$

$$\text{subsurface} = \left\langle \frac{1}{h}\Delta T\frac{\partial h}{\partial t}\right\rangle - \langle w\nabla_z T\rangle + \langle \nabla_z(\kappa\nabla_z T)\rangle_{z=-h}, \quad (2)$$

where $\nabla_H \equiv (\partial/\partial x, \partial/\partial y)$ and the other symbols are the same as in Eq. (1). The difference from the modified boundary flux form in Eq. (1) is that the advective tendency is a spatial average of the advection of local temperature gradient. Hereafter, Eq. (2) is referred to as a *local advection* form. When integrated over an entire volume of a domain, the local advection form produces an identical total advection to that given by the modified boundary flux form (Lee et al. 2004). However, the individual directional advective tendency differs between the two forms, as compared below. The contributions by all other components of the MLT balance (Fig. 11) are the same as those described for the modified boundary flux form (Fig. 8). All the tendencies are evaluated at hourly interval during the model's integration. Seasonal cycles of the local advection tendencies are consistent with those by Vialard et al. (2001). Below we analyze the nonseasonal component of the advective tendencies.

Most noticeably, the spatial average of local zonal advection warms the Niño-3 area during the 1998–99 La Niña while it is almost inactive during the 1997 El Niño (Fig. 11b). The anticorrelation between the advective tendency and Niño-3 MLT change does not describe the processes highlighted by the modified boundary flux form, that is, the large-scale warming process caused by the eastward advection of warm-pool water toward the cold tongue region (Fig. 8b; Picaut et al. 1997; WM01) and vice versa during a La Niña. Instead, the local zonal advection reflects the local warming in 1998–99 mainly by TIWs that are merely redistributing heat within the Niño-3 domain (Fig. 12; Lee et al. 2004).

a. *Internal heat redistribution by low-frequency currents*

As demonstrated above, the spatial average of local advective tendencies can be dominated by advection associated with TIWs, the currents with scales smaller than that of the domain of interest. However, the local

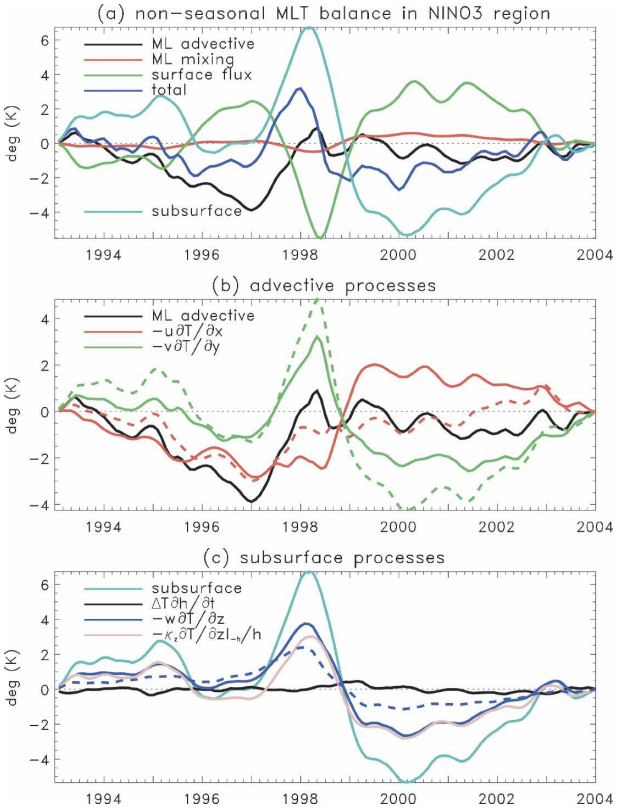

FIG. 11. Same as in Fig. 8, but that the advective tendencies are determined using the local advection form of Eq. (2). See Eq. (2) for notations. In (b) the tendencies are evaluated at two temporal resolutions using hourly (solid) and 30-day mean fields (dashed).

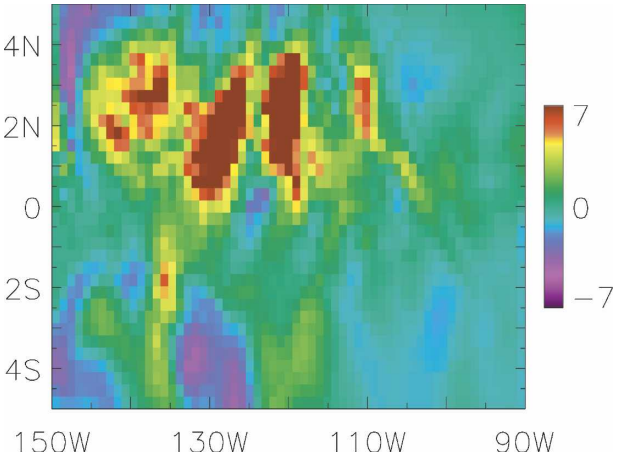

FIG. 12. Simulated zonal advective tendency evaluated with the local advection form ($-u\partial T/\partial x$) in December 1998, after depth averaging within an ML. Units are in K month^{-1}.

advective tendencies also contain the effect of advection by large-scale flow. In an attempt to separate tendencies associated with smaller-scales features such as TIWs from larger-scale current such as the equatorial zonal flow, previous studies (Vialard et al. 2001; WM01) have expanded velocity and temperature fields into high- and low-frequency parts (i.e., the so-called Reynolds decomposition). The rationale is that high-frequency features tend to have smaller scales whereas low-frequency signals usually have larger scales. Do advective tendencies associated with low-frequency, large-scale currents represent the large-scale, external advective processes described by the modified boundary flux formulation? This is an issue not addressed by Lee et al. (2004). Here we isolate the low-frequency, large-scale advection by computing advective tendencies using 30-day-averaged velocity and temperature fields, which effectively filters out the contributions by TIWs as they have a dominant period of about 20 days. We refer to these as low-frequency advection.

Figure 13 compares the low-frequency advection in zonal, meridional, and vertical directions evaluated using the modified boundary flux form (black curves) and by spatially averaging the local advective tendencies (gray dashed curves). If the two curves are close to each other, that means the spatial average of the local advective tendencies is able to represent the external heat source/sink as described by the modified boundary flux

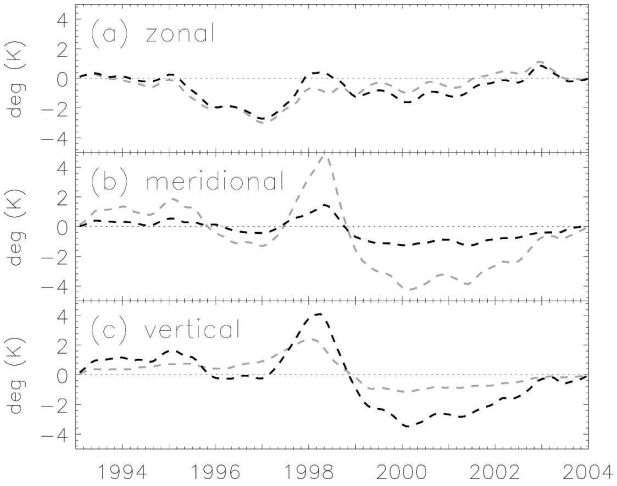

FIG. 13. The time integral of low-frequency advective tendencies in the (a) zonal, (b) meridional, and (c) vertical, evaluated using the modified boundary flux (black curve) and the local advection (gray curve) methods over the Niño-3 domain. The 30-day mean velocity and temperature fields are used to compute the tendencies. In evaluating the boundary flux tendencies in (a) and (b), the flux through the induction boundaries (i.e., between a mixed layer and a thermocline) is also included. This inclusion makes the dark curves in this figure differ slightly from the sums of the dashed curves shown in Figs. 9a,b. The gray curves are replicas of the dashed curves in Figs. 11b,c.

formulation. If the two curves are different, the spatial average of the local advection has significant contributions from internal redistribution of heat by low-frequency currents.

In the zonal direction (Fig. 13a), the advective tendencies evaluated by the two different formulation are very close to each other. Therefore, the low-frequency zonal advection evaluated by the local advective tendency describes the effect of currents that encompass the entire Niño-3 domain. This is because the anomalous surface zonal flow–associated El Niño and La Niña events span a larger zonal extent than the width of the Niño-3 region. In the meridional and vertical directions (Figs. 13b,c), the differences between the black and gray curves become much more substantial, reflecting the more dominant effect of internal heat redistribution within the Niño-3 box in these two directions by low-frequency currents. These are understandable for reasons described in the following. In the meridional direction, the low-frequency meridional Ekman flow has a scale that is smaller than the meridional extent of the Niño-3 box: the meridional Ekman flow changes sign across the equator, and their magnitude changes substantially between 0° and 5°N(S), the boundaries of the Niño-3 box. In the vertical direction, the magnitude of low-frequency upwelling attenuates significantly from the base of the mixed layer to the surface; in other words, the vertical scale of the upwelling is not larger than the depth of the mixed layer. From the similarities and differences of the black and gray curves seen in Fig. 13, we conclude that the local advection may describe the external advective heat source/sink for the Niño-3 region in the zonal direction by focusing only on low-frequency signals. This is not the case in the meridional and vertical directions because the scales of the flow in the respective direction are smaller in comparison with the corresponding extent of the Niño-3 mixed layer domain.

A general statement can be made from the above analysis. As long as a low-frequency current has a scale smaller than a domain of interest, internal redistribution may occur (such current will be hereafter called a low-frequency subdomain-scale current). As another example, let us consider the entire equatorial Pacific surface layer. There is no zonal advection of heat across the west and east land boundaries, based on the modified boundary flux method. However, the spatial average of low-frequency local advection describes the westward surface current advecting cold tongue water toward the warm pool. This creates a nonzero (rather large) zonal advective tendency that merely reflects internal heat redistribution within the equatorial Pacific. Again, the spatial scale of the zonal current is not large enough in comparison with the domain size.

As we briefly mentioned earlier, some previous studies have applied Reynolds decomposition to characterize the relative contribution of low- and high-frequency advection in the Niño-3 region using the spatial average of local advective tendencies. How well do these previous analysis compare with our result based on the same method of evaluating advective tendency? The low-frequency, local advective tendencies in Figs. 13a,b are consistent with Vialard et al. (2001, their Fig. 11d) and Niiler et al. (2004) in that the zonal and meridional tendencies generally assist the MLT change and the meridional tendency is larger than the zonal one. Niiler et al. further applied Reynolds decomposition, which may compare with our decomposition results made with the boundary flux analysis. Both Niiler et al. and our studies (our Fig. 10) report that the mean current advection of the temperature anomaly dominates the meridional advective tendency. Yet the dominance of the mean *zonal* current advecting the anomaly temperature in Niiler et al. does not agree with our boundary flux result. Niiler et al. used $5° \times 1°$ resolution observations while we use $1° \times 0.3°$ resolution. Niiler et al.'s balance is for "SST" at 15-m depth while we describe MLT. Also their local advection approach and our boundary flux approach may lead to different findings, as we described in this section. To make a more relevant comparison, we need to apply their method of spatiotemporal averaging to look at the 15-m-depth temperature, which is beyond the scope of this study.

b. Internal heat redistribution by eddies

In the zonal direction, eddy redistribution is significant, as described earlier with Fig. 12 and by Lee et al. (2004). Here we further quantify the relative role of internal heat redistribution by eddies and low-frequency subdomain-scale currents. The internal redistribution is computed as local advection tendency minus boundary flux tendency and its estimates are summarized in Table 2. The redistribution by low-frequency subdomain-scale zonal currents tends to be small, while the redistribution by eddies is larger during the 1998–99 La Niña period.

In the meridional direction, the spatial structure of eddy redistribution in the Niño-3 region (Fig. 14) shows that during the 1998–99 La Niña the tendency is positive at the equator, but it is negative away from the equator. These features are the result of TIWs redistributing heat meridionally. Because the warming effect at the equator overwhelms the cooling effect off the equator, the Niño-3 average of the local eddy meridional advection has a warming tendency during the La

TABLE 2. Internal redistribution of heat within the Niño-3 domain by low-frequency subdomain-scale currents and eddies, computed as a time integral of the local advection tendency minus the boundary flux tendency. The tendencies associated with the low-frequency subdomain-scale currents are shown in Fig. 13 after a time integral. The eddy tendency is the hourly evaluation of advective tendency minus the 30-day evaluation, shown in Figs. 11b,c (local advection approach) and Fig. 9 (boundary flux approach) after a time integral. As expected, the redistribution in the three directions adds up to 0. Units are K.

	1997–98 El Niño (Jan 1997–Mar 1998)		1998–99 La Niña (Mar 1998–Dec 1999)	
	Low frequency	Eddy	Low frequency	Eddy
Zonal	−1.0	−1.7	1.9	3.8
Meridional	4.2	−1.6	−6.4	3.5
Vertical	−3.2	3.2	4.4	−7.4

Niña (Table 2). The absence of such "warming" by TIWs during the corresponding El Niño results in the apparent anomalous "cooling" relative to the mean seasonal cycle. However, the redistribution by the eddies is smaller than that of the larger-scale subdomain-scale currents (Table 2).

In the vertical direction, the eddy redistribution during the 1998–99 La Niña is by far the largest among all the redistributing agents (Table 2). Let

$$-\int_{-h}^{0} \tilde{w}\frac{\partial \tilde{T}}{\partial z}\,dz = \tilde{w}(-h)\tilde{T}(-h) + \int_{-h}^{0} \frac{\partial \tilde{w}}{\partial z}\,\tilde{T}\,dz,$$

where the tilde denotes an eddy-associated anomaly. We assumed $\tilde{T}_r \approx 0$ because T_r is a domain mean and would be a low-frequency signal. TIW-related vertical velocity is the largest at about 60-m depth in this area, and diminishes to zero at the surface. Therefore, $\partial\tilde{w}/\partial z$ is nonzero and the eddy vertical tendencies evaluated by the two methods would differ from each other. In fact, while the boundary flux method produces a warming effect by the eddy vertical tendency (e.g., in 1998 of Fig. 9c; see also section 3), the local advection method presents a cooling effect (Fig. 11c). The cooling tendency is shown as well by Menkes et al. (2006) who used the local advection approach. The vertical eddy cooling tendency is a characteristic of the local advection method.

c. *Local advection tendency versus boundary flux tendency*

Now let us compare the total (eddy plus low frequency) local advective tendency with the modified boundary flux tendency for the 1997–99 El Niño/La Niña, to examine if the former can describe the external heat source/sink represented by the latter. The spatial average of local zonal advective tendency does not describe the warming process caused by the eastward advection of warm-pool water toward the cold tongue region during the 1997 El Niño and vice versa during the La Niña (Lee et al. 2004). In the meridional direction, local advective tendency varies by about 5 K during the 1997–99 El Niño/La Niña (Fig. 11b, solid green curve), significantly larger than the external contribution of about 2 K (Fig. 8b). Local vertical advective tendency contributes to the MLT change by about 6 K during the 1997–99 El Niño/La Niña (Fig. 11c), which is larger than about 3-K contribution by the external vertical heat exchange (Fig. 8c). The difference arises most notably because the local advection lacks the 4-K external warming effect by the eddies during the La Niña (shown in Fig. 9c).

The comparison of the advective tendencies between local advection and modified boundary flux methods indicates that, for all three directions, the spatial average of the local temperature advection cannot be interpreted as the external processes that control the temporal change of the Niño-3 MLT. The comparison also suggests that currents with scales smaller than the Niño-3 domain such as the eddies and the low-frequency subdomain-scale currents are very important in redistributing heat within the Niño-3 domain. Yet such internal redistribution is not very helpful in understanding the interannual variation of the Niño-3 volume-mean MLT. Our finding with regard to the difference between local advection and modified boundary flux approaches has implications not only to the Niño-3 region, but to many other areas as well (e.g., midlatitude regions that have eddies within).

Our findings about the advective mechanism of the Niño-3 MLT balance differ from Vialard et al. (2001). They concluded that surface heat flux, subsurface processes, and eddies (TIWs) are three major terms controlling interannual changes in spatial-mean MLT (their Fig. 11d). Although our local balance analysis would have led to a similar conclusion (our Fig. 11), our boundary flux approach has shown that surface heat flux, subsurface processes, and large-scale horizontal advection are the main contributors (Fig. 8a; Table 1). TIWs significantly influence only the vertical advective contribution to the MLT change, yet they are secondary to the effect of the large-scale upwelling (section 3).

5. Concluding remarks

We have analyzed the interannual balance of Niño-3-averaged mixed layer temperature (MLT) for the period of 1993–2003 using an ocean data assimilation

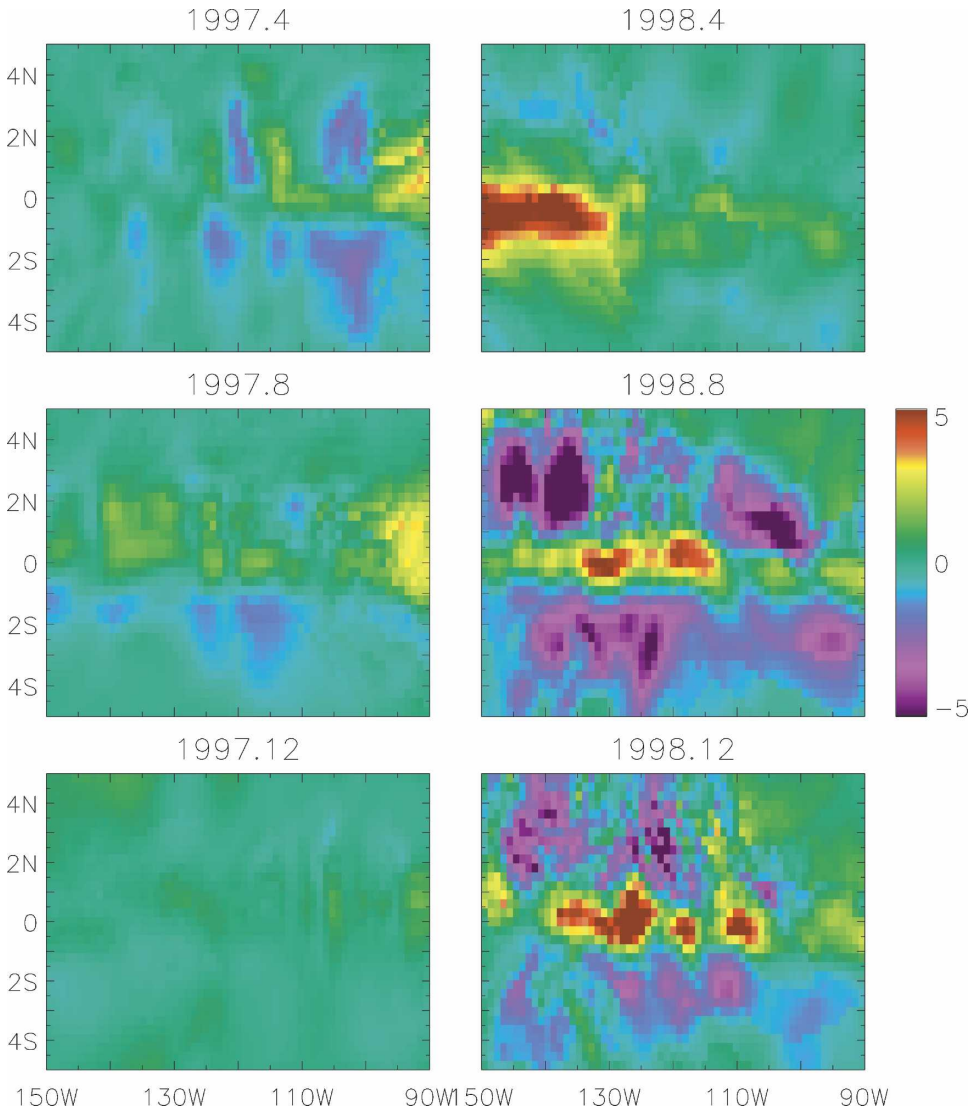

FIG. 14. Same as in Fig. 12, but for the meridional advective tendency ($-v\partial T/\partial y$). Units are in K month^{-1}. The numbers 4, 8, and 12 correspond to April, August, and December, respectively.

product. The objective is to understand the processes controlling the MLT in the Niño-3 region as a whole. We employed two newly developed methods to facilitate the analysis. The first method is a *modified boundary flux* formulation to evaluate external advective processes (Lee et al. 2004), where advective components of the MLT balance are evaluated as contributions through the boundaries of a domain. The second method is the discrete formulation of the entrainment heat advection (Kim et al. 2006), which allows us to close the MLT budget exactly using the z-coordinate model output.

The overall balance of the Niño-3-averaged MLT is such that the surface heat flux opposes the MLT change while the horizontal advection and the subsurface processes assist the change (section 3; Fig. 8). This overall balance applies to all three El Niño/La Niña events covered by the period of the study (1994–95, 1997–99, and 2002–03). The zonal advection is primarily associated with the eastward intrusion and westward retreat of the warm-pool water across the western boundary of the Niño-3 region in response to the trade wind anomaly (Fig. 9a). The meridional advective tendency is characterized by the mean-seasonal Ekman current advecting the large-scale temperature anomaly through the southern boundary of the Niño-3 domain (Figs. 9b and 10). The subsurface tendency is determined mostly by vertical mixing and vertical advection. As the thermocline temperature rises during El Niño events the vertical mixing weakens and produces warming tenden-

cies, and vice versa during La Niña events. The vertical advective tendency is contributed by changes in large-scale wind-driven upwelling as well as by tropical instability waves (TIWs). The two effects counteract each other, with the large-scale effect being larger by a factor of 2 (Fig. 9c). The entrainment heat advection associated with the temporal ML depth variation ($\Delta T \partial h/\partial t$) has a negligible effect on the MLT balance relative to other subsurface processes.

The modified boundary flux approach for evaluating the advective tendency leads to a conclusion that the dominant terms of the balance are surface heat flux, large-scale horizontal advection, vertical advection, and vertical mixing at the ML base (Table 1). All three advective contributions are primarily caused by large-scale processes. Moreover, the three advective tendencies are in phase with the MLT change.

In comparison, the spatial averages of the local advection of temperature (*local advection* approach) do not well depict the large-scale and external advective processes that control the averaged MLT of the Niño-3 domain. According to the local advection approach (section 4), the zonal advective tendency is anticorrelated with the change of MLT during the 1997–99 El Niño/La Niña events (Fig. 11), disagreeing with the common understanding about the role of large-scale advection of the warm-pool water during ENSO. The local advective tendency could be dominated by internal redistribution of heat by the currents with spatial scales smaller than the Niño-3 domain such as TIWs and low-frequency (lower than TIWs') currents. These currents merely redistribute heat within the Niño-3 domain. However, such redistribution does not serve as a heat source that warms the Niño-3 region.

Continuous and complete observations along the boundaries of a large domain are impractical or even impossible, making the application of the modified boundary flux approach difficult with observational data. In comparison, pointwise time-series measurements (e.g., by the TAO moorings) allow the application of the local advective method. Despite the limitations described above, when properly interpreted, the local advection approach may provide valuable insights on a local process that could reflect large-scale balance (e.g., the low-frequency zonal advective tendency).

The effects of TIWs on MLT balance (especially in terms of the various budget terms) have not been well documented. Our analysis suggests that TIWs do not have a dominant direct contribution to the interannual balance of MLT in the Niño-3 region as a whole. However, they are critical in redistributing heat within the Niño-3 region. Moreover, they may influence MLT balance indirectly by affecting air–sea heat exchange (Jochum et al. 2005 for a tropical Atlantic example). However their study suggests that oceanic heat gain from the atmosphere induced by TIWs is compensated by subsurface heat loss through entrainment, leaving the net effect of TIWs on the MLT budget small.

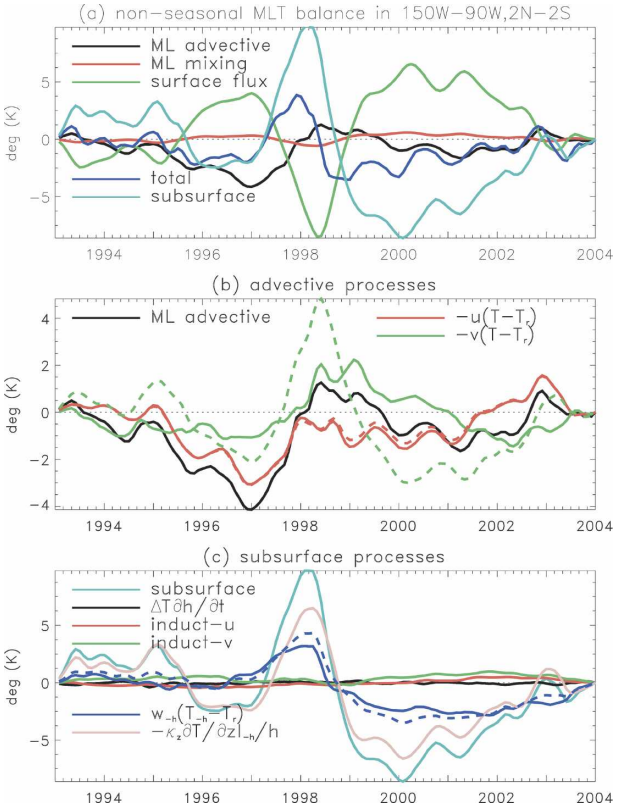

FIG. 15. Same as in Fig. 8, except that the domain is bounded by 2°N–2°S, 150°–90°W. The advective tendencies are evaluated using the boundary flux form. The solid (dashed) curves for the advective tendencies in (b) and (c) correspond to evaluations using hourly (30-day mean) fields.

We have concluded that the advective processes that control the averaged MLT of the Niño-3 region on an interannual scale are mostly large scale in nature. Does our conclusion depend on the area of the study (e.g., a smaller or larger region than Niño-3)? To examine this issue, the MLT budget is analyzed using the boundary flux form for an area defined by 2°N–2°S, 150°–90°W (Fig. 15), noting that TIWs have the largest effects on the MLT budget along these meridional boundaries (Figs. 12 and 14). The zonal advective tendency is hardly affected by the eddies. On the other hand, the eddies have a sizable warming effect through the meridional boundary in 1998 (Fig. 15b). Most of this warming is from north of 2°N toward the equator (i.e., the region north of 2°N experiences cooling in late 1998 as shown in Fig. 14). Thus, when the boundaries of the study intersect the eddies, TIWs become important.

The eddy warming via the vertical advective tendency of the 2°N–2°S box (Fig. 15c) is not as strong as the Niño-3 case (Fig. 9c) because the area of the strong eddy activity (2°–4°N) is excluded. Interestingly the net effect of the eddies on the MLT budget is similar for the 1998–99 La Niña between the Niño-3 and 2°N–2°S areas (cf. the eddy contributions between Figs. 9 and 15). Part of the heat transferred from the 2°–4°N band into the equatorial band comes from the TIW-induced vertical advective warming tendency in the 2°–4°N band. In other words, there is some compensation of eddy-induced meridional and vertical advective tendencies within the Niño-3 domain. This finding is qualitatively consistent with that of Jochum et al. (2004, their Fig. 15) for TIWs in the tropical Atlantic. To summarize, the individual advective tendencies are sensitive to the study area as a result of the eddy effects, but the total of the three advective tendencies is less sensitive to the choice of areas. Finally, we note that the Niño-3 area is analyzed in this study because its temperature is widely used as an index to diagnose changes associated with ENSO. Our findings help us to understand the processes responsible for the change of this index.

Acknowledgments. We thank Drs. Moto Nakamura and Benyang Tang for implementing the tendency output of the model, Dr. Zhangfan Xing for producing the model output, and the TAO Project Office for providing the observation data. Valuable comments by the reviewers and discussions with Dr. Xiaochun Wang greatly helped the manuscript. S.-B. Kim was supported in part by the Remote Sensing Systems. This study is a contribution of the consortium for the Estimating the Circulation and Climate of the Ocean (ECCO) and was carried out at the Jet Propulsion Laboratory, California Institute of Technology, under a contract with the National Aeronautics and Space Administration (NASA).

APPENDIX A

Local MLT Balance at 0°, 140°W and 0°, 110°W

To further evaluate the fidelity of the assimilation product, we examine the consistency of the simulated local MLT balance at the two TAO mooring locations with the observational analysis of WM01. The MLT balance at a point location can be written as (Kim et al. 2006)

$$\frac{\partial [T]}{\partial t} = \left[\frac{1}{\rho C_p}\frac{\partial q}{\partial z}\right] + \frac{1}{h}\kappa \nabla_z T|_{z=0} - [(u, v)\cdot \nabla_H T] + \text{subsurface} + [\text{ML mixing}] \quad \text{(A1)}$$

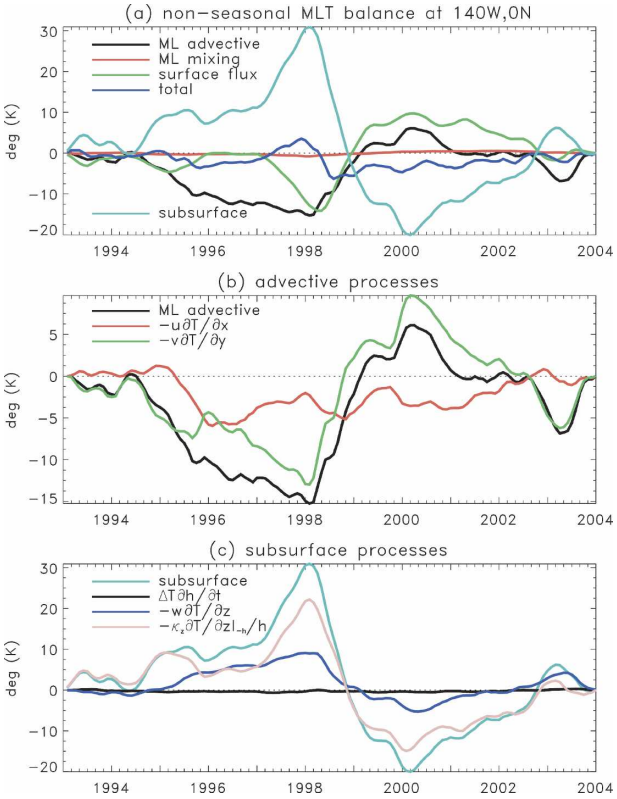

FIG. A1. Nonseasonal MLT budget, defined in Eq. (A1), at TAO mooring location at 0°, 140°W. See Eq. (A1) for notations.

with

$$\text{subsurface} = \frac{1}{h}\Delta T\frac{\partial h}{\partial t} - [w\nabla_z T] - \frac{1}{h}\kappa \nabla_z T|_{z=-h},$$

$$\Delta T = [T] - T_{-h},$$

where the square brackets represent the depth average within the ML. Note that ΔT is not the same as that for the volume-mean balance in Eqs. (1) and (2). Other notations are the same as in Eqs. (1) and (2). The MLT budget closes precisely as demonstrated in Kim et al. (2006). The advective tendency is computed at an hourly interval during the model integration, thus retaining high-frequency components.

Figures A1 and A2 describe the MLT balance, Eq. (A1), in a time-integrated form (from January 1993). The local MLT balance at the two mooring locations inferred from the model are generally consistent with that reported by WM01's observational analysis for the 1997–99 El Niño/La Niña. Surface heat flux opposes the MLT changes (Figs. A1a and A2a), while subsurface processes assist the changes (Figs. A1c and A2c). The mechanisms for the surface heat flux and the subsurface tendencies are very similar to those for the MLT aver-

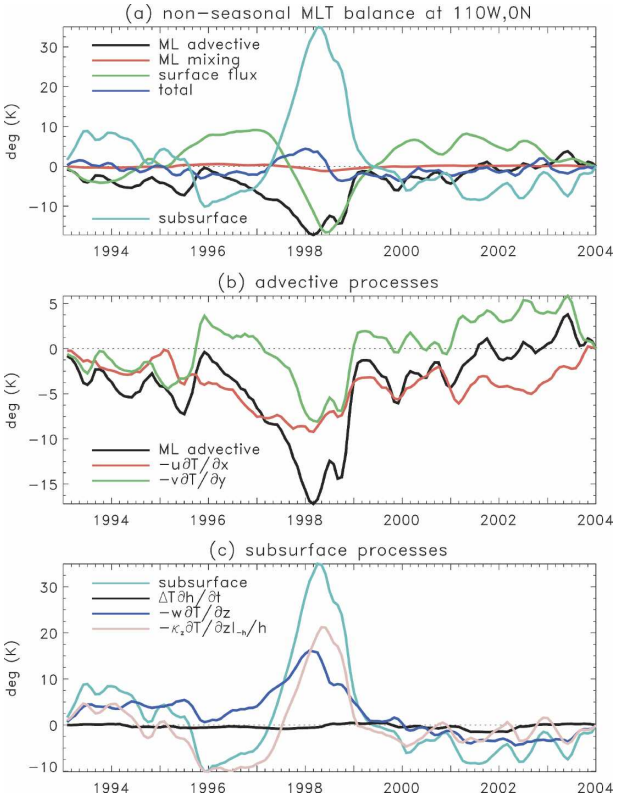

FIG. A2. Same as in Fig. A1 but for 0°, 110°W.

aged over the Niño-3 domain, thus, one may refer to section 3 for a detailed explanation of the mechanisms.

Zonal advective tendency contributes to a weak warming of the ocean at 0°, 140°W from late 1996 to late 1997 (Fig. A1b), but has a slight cooling tendency at 0°, 110°W in 1997 (Fig. A2b). Both contributions are smaller than the subsurface processes at both locations. Meridional advective tendency is negatively correlated with the MLT change (Figs. A1b and A2b). The anticorrelation reflects the warming effect of TIWs in late 1998 and their absence during 1997.

Results described above are in general agreement with WM01, except for the cooling by the zonal advection at 0°, 110°W in 1997. This difference is due to discrepancies in how gradients are evaluated. WM01 used a 4° differencing scheme while we use a 1° scheme. Our results become comparable to WM01's when their differencing scheme is used. Their scheme was not adopted here because it does not permit the closure of MLT budget.

The reasonably good agreement with WM01 in terms of the local MLT balance mechanism encourages us to analyze the MLT balance over the entire Niño-3 region, as described in section 3.

APPENDIX B

Seasonal MLT Balance

Here we evaluate the seasonal balance of the Niño-3 MLT using the boundary flux form. The seasonal cycles of tendencies are compiled by averaging the raw tendencies during the 1993–2003 period. The MLT has a warming tendency from September to March and correlates highly with the surface flux tendency (Fig. B1a). The surface flux tendency is positive with the peak in March (Fig. B1a). The shortwave incoming radiation dominates the surface flux but is modulated by cloud cover. The shortwave input has a semiannual cycle with peaks in March and October. Around October the cloud cover is greater than in March, resulting in the March peak in the shortwave input and the surface flux (Kessler et al. 1998).

The horizontal advection has a cooling tendency throughout the year, with both the zonal and meridional advection cooling most of the year (Fig. B1b). To examine the significance of the eddies in the horizontal advective tendencies, the tendencies are evaluated using 30-day-average values of temperature and velocity. The eddies explain about 50% of the meridional tendencies from November to January when the eddies are active (not shown), but in other months and in the zonal tendencies their contributions are negligible. Thus, the large-scale processes dominate the horizontal advective tendencies.

The zonal advective cooling reflects the westward advection of the cold tongue water. Taking warmer water in the western part of the Niño-3 domain westward out of the domain would leave the averaged temperature of the Niño-3 domain cooler, resulting in the cooling tendency. The advective cooling through the western boundary of the Niño-3 area is dominant over its eastern boundary counterpart (Fig. B1c). The spring weakening of the cooling tendency is clear in the western boundary flux and is a consequence of the weak easterlies in spring. According to other studies, the zonal advection even warms the eastern tropical Pacific in spring (Vialard et al. (2001) for the Niño-3 region; Kessler et al. (1998) for 2°S–2°N, 120°–90°W; Wang and McPhaden (1999) at the TAO mooring locations). These studies used the local advection form to evaluate the tendency. When we compute the zonal tendency using the local advection form, indeed we find the warming in spring (not shown).

The meridional advective cooling is the result of the poleward divergence within a mixed layer driven by the easterlies. One exception is the warming tendency around September across 5°N (Fig. B1c). The warming

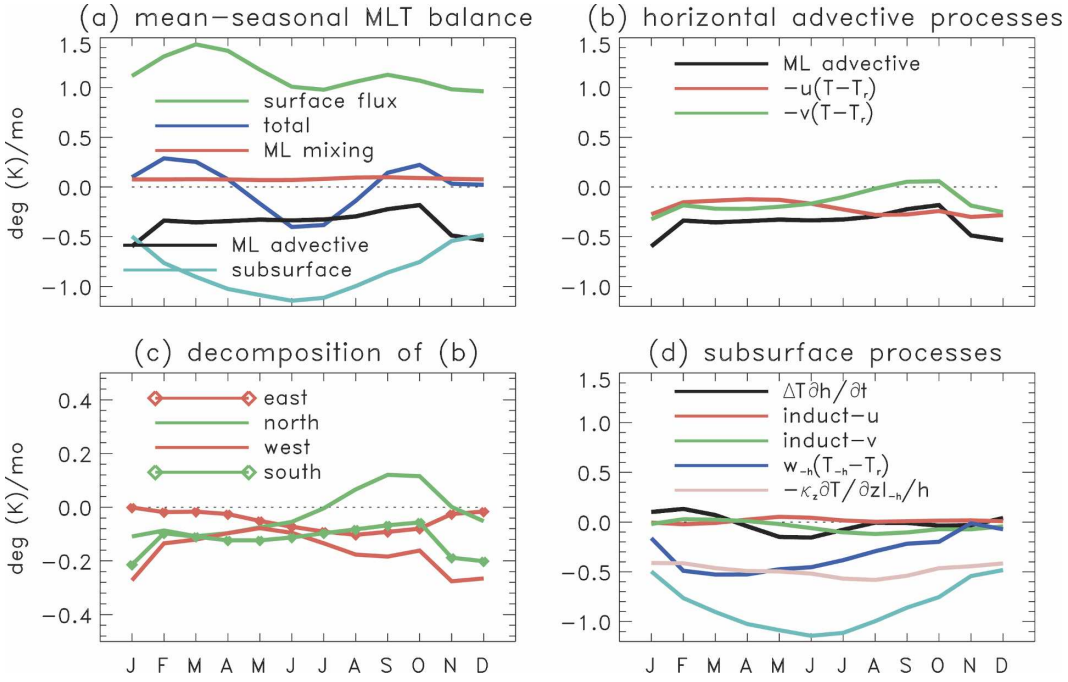

FIG. B1. Mean-seasonal MLT balance complied over 1993–2003 in the Niño-3 area: (a) overall balance, (b) advective processes within a ML, (c) advective tendencies through the four horizontal boundaries, and (d) subsurface processes. The tendencies are computed hourly, averaged over 30 days, and smoothed with a three-point (90 days) running mean. The advective tendencies are computed using the modified boundary flux form.

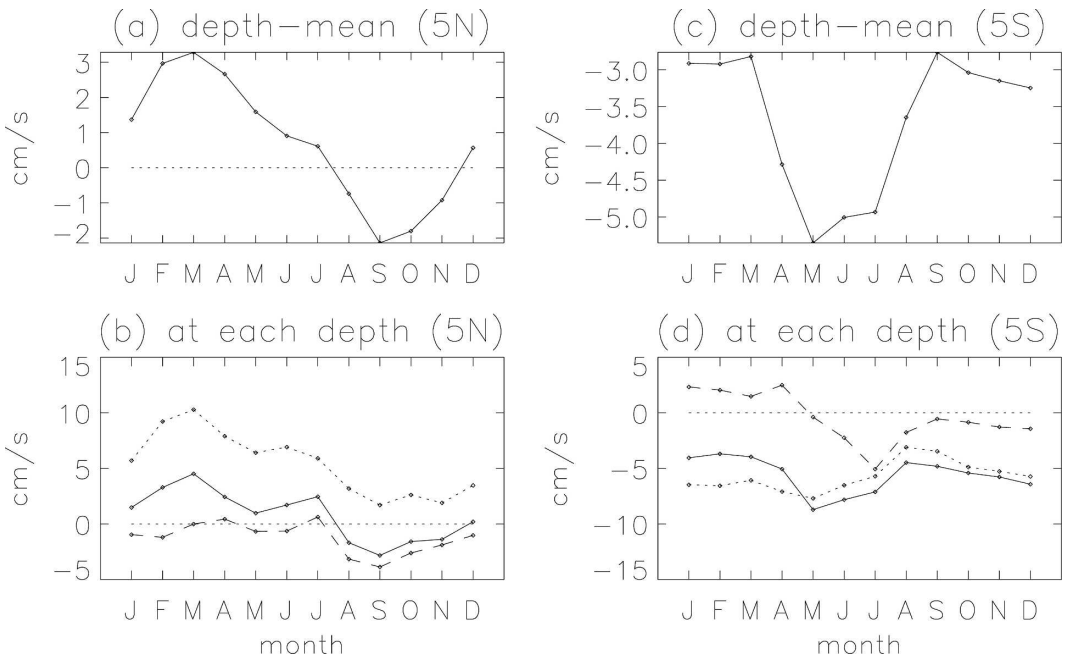

FIG. B2. Simulated seasonal meridional velocity at 5°N and 5°S, averaged between 150°–90°W and over the 1993–2003 period: (a), (c) the depth mean within a mixed layer; (b), (d) the velocities at depths of 5 (dotted), 25 (solid), and 45 m (dashed).

tendency in these months has to do with a southward flow within a mixed layer across 5°N (Fig. B2a). The southward velocity is a combined result of weak northward Ekman divergence and strong southward geostrophic flow. In detail, around September the northeasterlies near 5°N weaken (see the corresponding surface Ekman current in the dotted curve of Fig. B2b) as a result of the northward migration of the intertropical convergence zone (a spatially coherent wind pattern is found at 9°N, Fig. 9 of Kessler 2006). At the same time, the southward geostrophic flow strengthens (dashes in Fig. B2b). The seasonal strengthening of the geostrophic flow may be associated with the fall weakening of the vorticity barrier along 8°N that usually blocks the southward geostrophic flow across this latitude (Coles and Rienecker 2001). In summary, the weak zonal wind and the strong southward geostrophic flow are responsible for the September warming tendency by the meridional advection across 5°N. In comparison, the meridional velocity at 5°S within a mixed layer is predominantly divergent due to the strong easterlies (Figs. B2c,d), resulting in the cooling tendency throughout a year.

The seasonal subsurface tendencies are as follows (Fig. B1d). The vertical mixing at the ML base has a cooling tendency, resulting from the mixing with the cold thermocline water. The vertical advective tendency cools the Niño-3 domain throughout the year, indicating the large-scale upwelling. The cooling is the most intense in boreal spring and weak in fall and winter. This seasonality is due to the vertical advective warming by TIWs. When the tendency is evaluated using 30-day averages of temperature and velocity, the TIW-warming effect disappears [e.g., its curve becomes very close to that of the vertical mixing throughout the year (not shown)]. The warming by TIWs is consistent with the similar warming presented for the nonseasonal MLT budget in section 3. The other components of the subsurface tendency (i.e., $\partial h/\partial t$ and lateral induction) are relatively small.

REFERENCES

Barnier, B., L. Siefridt, and P. Marchesiello, 1995: Thermal forcing for a global ocean circulation model using a 3-year climatology of ECMWF analyses. *J. Mar. Syst.,* **6,** 363–380.

Boyer, T. P., and S. Levitus, 1998: *Objective Analysis of Temperature and Salinity for the World Ocean on a 1/4° Grid.* NOAA Atlas NESDIS 27, 62 pp.

Bryden, H. L., and E. C. Brady, 1985: Diagnostic model of the three-dimensional circulation in the upper equatorial Pacific Ocean. *J. Phys. Oceanogr.,* **15,** 1255–1273.

Coles, V. J., and M. M. Rienecker, 2001: North Pacific subtropical-tropical gyre echanges in the thermocline: Simulations with two isopycnic OGCMs. *J. Phys. Oceanogr.,* **31,** 2590–2611.

Cox, M. D., 1980: Generation and propagation of 30-day waves in a numerical model of the Pacific. *J. Phys. Oceanogr.,* **10,** 1168–1186.

da Silva, A. M., C. C. Young, and S. Levitus, 1994: *Atlas of Marine Surface Data.* U.S. Government Printing Office, 74 pp.

Fukumori, I., 2002: A partitioned Kalman filter and smoother. *Mon. Wea. Rev.,* **130,** 1370–1383.

——, 2006: What is data assimilation really solving, and how is the calculation actually done? *Ocean Weather Forecasting—An Integrated View of Oceanography,* E. P. Chassignet and J. Verron, Eds., Springer, 317–342.

——, R. Raghunath, L.-L. Fu, and Y. Chao, 1999: Assimilation of TOPEX/Poseidon altimeter data into a global ocean circulation model: How good are the results? *J. Geophys. Res.,* **104,** 25 647–25 655.

Gent, P. R., and J. C. McWilliams, 1990: Isopycnal mixing in ocean circulation models. *J. Phys. Oceanogr.,* **20,** 150–155.

Halpern, D., R. A. Knox, and D. S. Luther, 1988: Observations of 20-day period meridional current oscillations in the upper ocean along the Pacific equator. *J. Phys. Oceanogr.,* **18,** 1514–1534.

Hansen, D. V., and C. A. Paul, 1984: Genesis and effects of long waves in the equatorial Pacific. *J. Geophys. Res.,* **89,** 10 431–10 440.

Hayes, S. P., P. Chang, and M. J. McPhaden, 1991: Variability of the sea surface temperature in the eastern equatorial Pacific during 1986–1988. *J. Geophys. Res.,* **96,** 10 553–10 566.

Jin, F.-F., 1997: An equatorial recharge paradigm for ENSO. Part I: Conceptual model. *J. Atmos. Sci.,* **54,** 811–829.

Jochum, M., P. Malanotte-Rizzoli, and A. J. Busalacchi, 2004: Tropical instability waves in the Atlantic Ocean. *Ocean Modell.,* **7,** 145–163.

——, R. Murtugudde, R. Ferrari, and P. Malanotte-Rizzoli, 2005: The impact of horizontal resolution on the tropical heat budget in an Atlantic Ocean model. *J. Climate,* **18,** 841–851.

Kessler, W. S., 2006: The circulation of the eastern tropical Pacific: A review. *Prog. Oceanogr.,* **69,** 181–217.

——, L. M. Rothstein, and D. K. Chen, 1998: The annual cycle of SST in the eastern tropical Pacific, diagnosed in an ocean GCM. *J. Climate,* **11,** 777–799.

Kim, S. B., T. Lee, and I. Fukumori, 2004: The 1997–1999 abrupt change of the upper ocean temperature in the north central Pacific. *Geophys. Res. Lett.,* **31,** L22304, doi:10.1029/2004GL021142.

——, I. Fukumori, and T. Lee, 2006: The closure of the ocean mixed layer temperature budget using level-coordinate model fields. *J. Atmos. Oceanic Technol.,* **23,** 840–853.

Large, W. G., J. C. McWilliams, and S. C. Doney, 1994: Ocean vertical mixing: A review and a model with a nonlocal boundary layer parameterization. *Rev. Geophys.,* **32,** 363–403.

Lee, T., I. Fukumori, D. Menemenlis, and L.-L. Fu, 2002: Effects of the Indonesian Throughflow on the Pacific and Indian Oceans. *J. Phys. Oceanogr.,* **32,** 1404–1429.

——, ——, and B. Tang, 2004: Temperature advection: Internal versus external processes. *J. Phys. Oceanogr.,* **34,** 1936–1944.

Lukas, R., and E. Lindstrom, 1991: The mixed layer of the western equatorial Pacific Ocean. *J. Geophys. Res.,* **96,** 3343–3357.

Marshall, J. C., C. Hill, L. Perelman, and A. Adcroft, 1997: Hydrostatic, quasihydrostatic and non-hydrostatic ocean modeling. *J. Geophys. Res.,* **102,** 5733–5752.

McPhaden, M. J., 2004: Evolution of the 2002/03 El Niño. *Bull. Amer. Meteor. Soc.,* **85,** 677–695.

Meinen, C. S., M. J. McPhaden, and G. C. Johnson, 2001: Vertical velocities and transports in the equatorial Pacific during 1993–99. *J. Phys. Oceanogr.,* **31,** 3230–3248.

Menkes, C., J. Vialard, S. C. Kennan, J.-P. Boulanger, and G. Madec, 2006: A modeling study of the impact of tropical instability waves on the heat budget of the eastern equatorial Pacific. *J. Phys. Oceanogr.,* **36,** 847–865.

Niiler, P. P., D.-K. Lee, and J. Moisan, 2004: Observed mechanisms of El Niño SST evolution in the Pacific. *J. Mar. Res.,* **62,** 771–786.

Picaut, J., F. Masia, and Y. duPenhoat, 1997: An advective-reflective conceptual model for the oscillatory nature of the ENSO. *Science,* **277,** 663–666.

Qiu, B., 2002: The Kuroshio Extension system: Its large-scale variability and role in the midlatitude ocean-atmosphere interaction. *J. Oceanogr.,* **58,** 57–75.

Schiller, A., J. S. Godfrey, P. C. McIntosh, G. Meyers, and R. Fiedler, 2000: Interannual dynamics and thermodynamics of the Indo-Pacific Oceans. *J. Phys. Oceanogr.,* **30,** 987–1012.

Schopf, P. S., and M. J. Suarez, 1988: Vacillations in a coupled ocean atmosphere model. *J. Atmos. Sci.,* **45,** 549–566.

Vialard, J., and P. Delecluse, 1998: An OGCM study for the TOGA decade. Part I: Role of salinity in the physics of the western Pacific fresh pool. *J. Phys. Oceanogr.,* **28,** 1071–1088.

——, C. Menkes, J.-P. Boulanger, P. Delecluse, E. Guilyardi, M. J. McPhaden, and G. Madec, 2001: A model study of oceanic mechanisms affecting equatorial Pacific sea surface temperature during the 1997–98 El Niño. *J. Phys. Oceanogr.,* **31,** 1649–1675.

Wang, W. M., and M. J. McPhaden, 1999: The surface-layer heat balance in the equatorial Pacific Ocean. Part I: Mean seasonal cycle. *J. Phys. Oceanogr.,* **29,** 1812–1831.

——, and ——, 2001: Surface layer temperature balance in the equatorial Pacific during the 1997–98 El Niño and 1998–99 La Niña. *J. Climate,* **14,** 3393–3407.

Wyrtki, K., 1975: El Niño—The dynamic response of the equatorial Pacific Ocean to atmospheric forcing. *J. Phys. Oceanogr.,* **5,** 572–584.

Zebiak, S. E., and M. A. Cane, 1987: A model El Niño–Southern Oscillation. *Mon. Wea. Rev.,* **115,** 2262–2278.